Meteorol. Z. (Contrib. Atm. Sci.), Vol. **28**, No. 5, 389–415 (published online July 18, 2019)

Low Level Jets over the Southern North Sea

David Wagner[1,2*], Gerald Steinfeld[1], Björn Witha[1], Hauke Wurps[1] and Joachim Reuder[3]

[1]ForWind – Center for Wind Energy Research, University of Oldenburg, Germany
[2]now at WSL Institute for Snow and Avalanche Research SLF, Switzerland
[3]Geophysical Institute, and Bergen Offshore Wind Centre (BOW), University of Bergen, and Bjerknes Centre for Climate Research, Bergen, Norway

(Manuscript received October 17, 2018; in revised form April 3, 2019; accepted May 3, 2019)

Abstract

An extensive analysis of Low Level Jets (LLJs) over the Southern North Sea is presented. The study is based on observational data from a wind LiDAR and a passive microwave radiometer, operated from May 2015 to October 2016 on the FINO1 platform, as well as on mesoscale simulations by WRF-ARW. Besides evaluations on LLJ occurrence, intensity, direction, height, wind shears and boundary layer stability based on 250 days of measurements, two case studies were investigated in detail. It indicates that LLJs are a very frequent phenomenon above the Southern North Sea as they occurred on the majority of the days during the measuring period. Our study suggests that highest probabilities for LLJs to occur are during winds within the sector East to South. Most detections were found for the period between the evening until morning while the lowest amount of detections was found at 1400 UTC. Considerable amounts of LLJs occurred at heights that are in the ranges of modern offshore wind turbine heights and rotor sizes. Moreover, the case studies showed strong wind shears and veering below the jet cores. Further findings suggest, that baroclinic effects in the coastal zone due to differential surface heating of land and sea as well as inertial oscillations may form and modify these jets.

Keywords: Low Level Jets, LLJ, Southern North Sea LLJ, WRF, Offshore LLJs, FINO1, Baroclinicity, Inertial Oscillation

1 Introduction

Low Level Jets (LLJs) are wind maxima in the lower troposphere and were frequently investigated in the past. They can be crucial for supercell formation and tornadogenesis above the Great Plains (Coffer and Parker, 2015) as well as for aviation safety (Blackadar, 1957) due to strong low-level wind shears. LLJs are also known for transporting moisture (Chen and Tomassini, 2015) or pollutants (Angevine et al., 2006) over large distances. Over the time, the aspect of wind energy increased more and more in LLJ research (Högström and Smedman-Högström, 1984; Storm et al., 2009; Banta et al., 2013; Emeis, 2013; Vanderwende et al., 2015; Dörenkämper et al., 2015b), mainly as a result of their low altitudes, high wind speeds and high wind shears. These characteristics make LLJs interesting for wind energy meteorology research in terms of – most obviously – yield and wind farm planning but also for turbine loads due to their often high wind shears (Emeis, 2014; Gutierrez et al., 2016; Gutierrez et al., 2017). LLJ research in the wind energy context is especially interesting for regions with high densities of wind turbines. For Northern Europe, the German Bight can currently be named as one of the places with the highest offshore wind energy usage.

*Corresponding author: David Wagner, WSL Institute for Snow and Avalanche Research SLF, Flüelastrasse 11, 7276 Davos Dorf, Switzerland, e-mail: david.wagner@slf.ch

LLJs occur above both, land and sea, and can have different driving mechanisms, primarily inertial oscillations (IOs) and baroclinicity which itself is either a result of strong temperature gradients in the coastal zone, frontal passages or topographic effects (Lettau, 1954; Blackadar, 1957; Bonner, 1968; Högström and Smedman-Högström, 1984; Stull, 1988; Burk and Thompson, 1996; Song et al., 2005; Baas et al., 2010; Mahrt et al., 2014; Floors et al., 2015). The drivers may occur alone or can interfere with each other which makes the research of understanding LLJs complex. Blackadar (1957) observed nocturnal LLJs over land and developed a theory according to which LLJs form at the top of the nocturnal atmospheric boundary layer (ABL) as a consequence of sudden frictional decoupling due to fast ABL stabilization and the induction of IOs. However, this diurnal dependence of IOs is under discussion (Lundquist, 2003).

Högström and Smedman-Högström (1984); Smedman et al. (1993); Smedman et al. (1995); Smedman et al. (1996); Smedman et al. (1997b); Dörenkämper et al. (2015a), among others, investigated stable internal boundary layers (SIBLs) and LLJs above the Baltic Sea. They associated the occurrence of LLJs with the existence of SIBLs. As relatively warm, continental air travels from the land seawards over the coastline, an SIBL begins to form as a result of the relatively cool sea surface temperature (SST). This results in a sudden, quasi-frictional decoupling of the air aloft. Smedman et al. (1993) described the effect as a spatial analogy to the

theory developed by Blackadar (1957). The conditions favouring these LLJs over the Baltic Sea are mainly found during spring and summer (Smedman et al., 1996; Källstrand, 1998; Dörenkämper et al., 2015a). LLJs were found to occur in over 60 % of the time during spring (Smedman et al., 1996; Smedman et al., 1997a). Svensson et al. (2016) found clear seasonal differences in LLJ properties above the Baltic Sea, e.g. lower LLJ core heights as a consequence of more stable regimes during spring. Stable to very stable conditions above the North Sea occur less frequently compared to the Baltic Sea, as shown by Dörenkämper (2015). Following the theory, that LLJs mainly evolve under stable to very stable regimes, LLJs over the North Sea would be expected to be less frequent than over the Baltic Sea.

However, IOs are not the only drivers for LLJ formation. Mahrt et al. (2014) argued, that an IO may be important for the formation of observed LLJs off the East Coast of the United States, but cannot explain the quick formation of the wind maxima and the strong wind shears. Beardsley et al. (1987) and Burk and Thompson (1996) showed that baroclinicity in the coastal zone drives the southward LLJ along the Californian coast, where the jet core is embedded in a sloped marine ABL temperature inversion. They also found, that the baroclinic zone built an important environment for the LLJ, while IOs also contributed considerably to the formation. In those cases it was found that the baroclinicity was the reason for the lower wind speeds above the peak, while friction resulted in the lower wind speeds below the peak. Colle and Nowak (2010) and Helmis et al. (2013) present as well strong baroclinic dependencies of LLJs along the U.S. East Coast. LLJs may often form towards the coastline. However, in at least one case (Angevine et al., 2006), it was reasoned, that the LLJ occurred immediately as an IO response after the collapse of the sea-breeze circulation. Nearly all cited studies dealing with LLJs over the sea have in common, that they found the most of the LLJs occurring during the spring and summer months – mainly between March and June when the SST is still rather low and the land surface is considerably warmer during daytime.

To date, LLJs above the North Sea, and especially above its southern part, are relatively unexplored, though their understanding might be of relevance for offshore wind energy applications but also in the climatic, oceanographic and ecological context. Nunalee and Basu (2014), to name one of the few studies focussing on LLJs over the North Sea, investigated LLJs at FINO1 with WRF-ARW and found in general a good capability of the model to represent LLJs, although the intensity and wind shear was underestimated. Other studies found similar results concerning difficulties in representing these LLJ characteristics in WRF (Floors et al., 2013; Peña et al., 2014; Svensson et al., 2016; Yang et al., 2016). Tuononen et al. (2015) derived a climatology of LLJs for the northern hemisphere based on reanalysis data including the North Sea. Kalverla et al. (2017) investigated LLJs at the Ijmuiden met mast off the coast of Ijmuiden, the Netherlands. However, there is still a lack of detailed knowledge on LLJ properties and formation mechanisms for this area. Thus, as the Southern North Sea is one of the most important sites for offshore wind energy in Europe, knowledge about LLJs in this region is of great interest for a wide range of scientific and industry-relevant questions. Those include, to name a few, improved predictability of power production and system loads, wind farm layout, influences of LLJs on turbine wakes or mechanical loads induced by wind shear. The following study, based on both observations by state-of-the-art remote sensing techniques and model data, contributes to filling knowledge gaps and provides information on properties and formation mechanisms of LLJs above the Southern North Sea. The LLJ characteristics including LLJ core altitudes, frequency of occurrence, wind speeds, wind directions, wind shears and atmospheric stability are investigated based on 250 days of measurements. Two case studies are investigated in detail, based on the measurement data as well as model data from WRF-ARW. Based on these evaluations, possible formation mechanisms are suggested. With this knowledge, further remote sensing measuring campaigns of the MABL that investigate LLJs can be planned, with clearer foci and longer temporal extents at different sites.

In Section 2 we explain the methodology, i.e. the measuring site, model setup, considered data and the LLJ detection method. In Section 3, we introduce and discuss the results based on observation and model data, distributed into a data analysis part based on long-term measurements and a part containing two case studies. This is followed by a short conclusion and research outlook in Section 4.

2 Site and methodology

The observation data was obtained from instrumentation installed at the FINO1 offshore research platform (Neumann et al., 2003; Neumann et al., 2004), located about 45 km to the north of the German island of Borkum (54.014° N, 6.587° E, Figure 1). The base of the FINO1 platform is situated at a height of 20 m above mean sea level (AMSL) while the top of the mast reaches 101 m AMSL. Our area of investigation with the mesoscale model WRF covers large parts of the Southern North Sea and the surrounding landmasses and is introduced in detail in section 2.4. As shown in Figure 1, no noteworthy terrain elevations occur in this area. We can therefore exclude a significant influence of the terrain on LLJs over and close to the coastlines of Denmark, Northern Germany, North-Western Germany and the Netherlands. The prevailing wind direction at FINO1 is South-West (Beeken and Neumann, 2008). Coastal upwelling due to Ekman transport of cooler water from lower ocean layers may enhance the temperature contrast between land and sea in coastal zones with deeper waters and therefore effect the LLJ persistence and intensity (Beardsley et al., 1987; Soares et al., 2014).

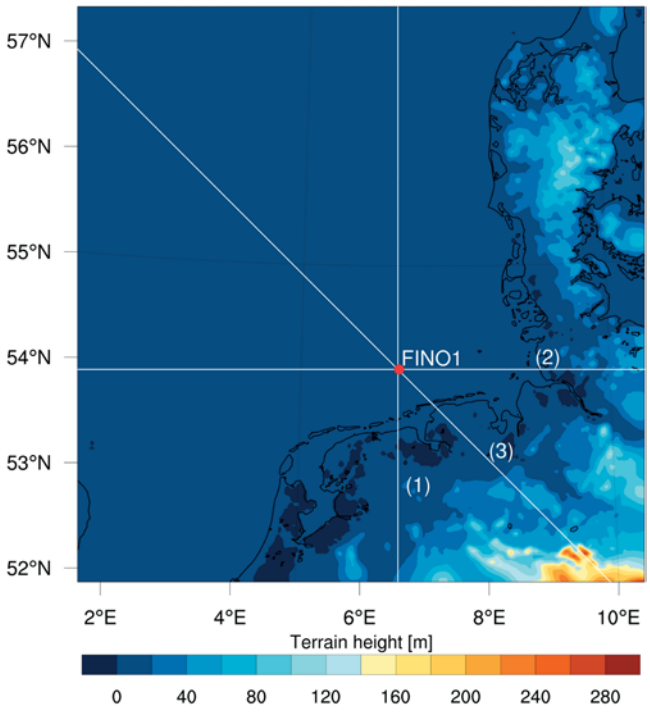

Figure 1: Terrain height map of domain 3 (D3) of the WRF output. The white lines mark the vertical cross section cuts related to Figure 15, 16, 25 and 26. FINO1 is located at their intersection (red dot).

However, due to the shallowness of the Southern North Sea, wind-driven upwelling of cold water can be neglected in this area (Lee, 1980). The Southern North Sea is an important development area for offshore wind energy with several wind farms in the vicinity of FINO1. This has impacts on wind measurements, as will be addressed in the next section.

2.1 Observation data

From the sensors which are permanently mounted on the met mast, we used data from the cup anemometers and wind vanes from 33 m up to 60 m AMSL (Table 1). From temporally installed instruments on the platform, we used data from a Windcube© 100s wind LiDAR (e.g. Kumer et al., 2014) and a RPG-HATPRO-G4 passive microwave radiometer (Radiometer Physics, 2015). These two remote sensing instruments were installed as part of the OBLEX-F1 measurement campaign, which was conducted in the period from May 2015 to September 2016 (Cherukuru et al., 2017; Krishnamurthy et al., 2017; Bakhoday Paskyabi et al., 2017). The OBLEX-F1 campaign aimed to enhance the understanding of the offshore ABL at FINO1 with the help of several measuring instruments installed at the platform, i.e. wind LiDARs, a passive microwave radiometer or ultrasonic anemometers.

2.1.1 Wind data

From the Windcube© 100s wind LiDAR we used the horizontal and vertical wind vector components obtained from measurements in pulsed Doppler Beam Swing (DBS) scan mode (Wagner and Courtney, 2010). The maximum measuring height of the LiDAR was 3126 m. However, as our study focussed on LLJs with cores at heights where they may affect offshore turbines, we used the LiDAR measuring range from 72 m up to 518 m AMSL for our study. In 2017, newly installed offshore turbines had an average hub height of 96 m and an average rotor diameter of 136 m (Fraunhofer IWES, 2018). The effective vertical resolution of the LiDAR was 23.5 m. The dataset is discussed in detail below. The detection period for the LiDAR was from 22 May 2015 to 30 April 2016 (345 days) but for the complete October 2015, large parts of September and November 2015, as well as for parts of June 2015 no data from the LiDAR was available (Figure 2, Table 3). The total LiDAR data availability at a height of 213 m (which is the height, where the availability of LiDAR data is highest) is 11.9 % after preprocessing for the whole period of 345 days. This low availability is a consequence of time-discontinuous LiDAR measurements and partial instrument failure. However, there are reasons why we think that the amount of data justifies an evaluation: To our knowledge, there is no comparable study over this time-span at FINO1 that considers LLJs. Indeed, there was a relatively low data availability over the whole time period. The reason for this was that the device was over a long time in a mode where it recorded every 2 hours for 20 minutes in a row instead of recording continuously (Figure 3). However, as LLJs occur generally over several hours, these periods are sufficient to detect LLJs, although in less detail. At 518 m height, the data availability in relation to this whole measuring period was 10.6 % (Figure 2).

As addressed above, the LiDAR was running in DBS mode during our measurements. In this mode, one measurement at a fixed elevation angle of 70° for each azimuth angle was conducted every 2–5 seconds. The azimuth angles were 0°, 90°, 180° and 270°. A DBS "round" containing measurements for all 4 azimuth angles was completed after 15–18 seconds. For each round, the wind speed components u, v and w were computed. This resulted in 30–40 records per 10 minute interval. We excluded 10 min intervals when a critical threshold of 10 records was not reached. This results in a minimum data availability of at least 25 % for each 10 min averaging window. Before averaging of the LiDAR data, we applied a critical threshold of 3σ ms^{-1} for the deviation of the mean to exclude outliers. Additionally, records which were outside the Carrier-to-Noise

Table 1: Data used to detect LLJs. For each parameter, the time resolution is 20 min (avg).

Sensor	Parameter	Heights (m AMSL)
Wind LiDAR	u,v,w	72–518, every 23.5
Microwave radiometer	T	25 –525, every 25
Cup Anemometer	ws (u, v)	33, 40, 50, 60
Wind vane	wd (u, v)	33, 40, 50, 60

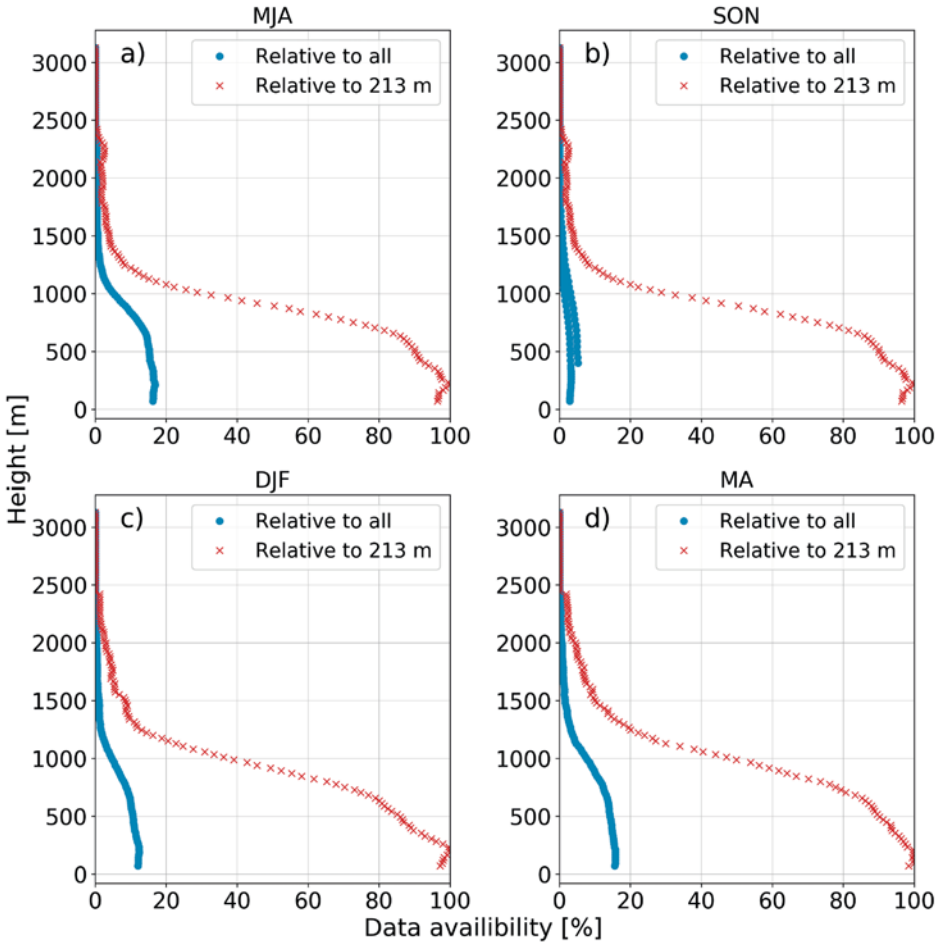

Figure 2: LiDAR data availability during (a) May–August 2015, (b) September–November 2015, (c) December 2015–February 2016 and (d) March–April 2016. The blue dots mark the data availability on all 345 days the LiDAR was installed between May 2015 and April 2016. The red dots mark the data availability relative to the highest count of data points at 10 min time stamps for each period.

Ratio (CNR) interval $[-25, 5]$ dB, were excluded from the further analysis. The lower limit of −25 is slightly below the recommendations of the LiDAR manufacturer Leosphere given as −22, but has empirically been proven to result in reliable wind measurements under the conditions during the OBLEX-F1 campaign, thus providing us with an extended data set for our analysis. The upper limit of +5 was chosen to exclude measurements close to clouds. The water droplets within clouds lead to refraction of the LiDAR laser beam, which in turn would cause erroneous detections of the wind vectors.

10 min averages of the measured data were calculated. The time stamps denote the start of each averaging period. The data obtained from the cup anemometers, which was already quality-checked, was additionally corrected for mast shadow effects using the correction algorithm from Westerhellweg et al. (2012). Note that the availability and range of LiDAR data also strongly depend on the concentration of the aerosol particles which reflect the emitted laser beam. It was furthermore shown by Platis et al. (2018) that wind farm wakes may persist several tens of kilometers behind wind farms under stable regimes. Thus, wakes could affect the FINO1 observations for several wind directions. Especially the wakes of the Alpha Ventus wind farm, only 400 m to the East, should be considered. We experienced correlations between the LiDAR and cup anemometer data at both 70 m and at 100 m of $r = 0.96$. This value does not appear particularly good, however due to the proximity of the LiDAR device to the mast and the fixed elevation angle of 70°, it is expected that the DBS scan is affected by the mast to a certain degree which we could not quantify yet. Kumer et al. (2014) found an correlation of $r = 0.95$ in comparisons with radiosondes up to 1590 m, however measured at the airport of Stavanger, Norway.

An issue concerning the detection of LLJs was that the lowest measurement level of the LiDAR was at 72 m height. As offshore LLJs can occur at heights below this level (Smedman et al., 1995), we combined data of cup anemometers and wind vanes below 70 m, with the LiDAR data from the levels above. By that we obtained wind profiles with 25 discrete height levels between 33 m and 518 m (Figure 3). The distances between levels depend on whether the levels correspond to a cup anemometer measurement (7 to 10 m) or LiDAR measurements (23.5 m range gates) (Table 1). The transition between cup anemometer and LiDAR measurement

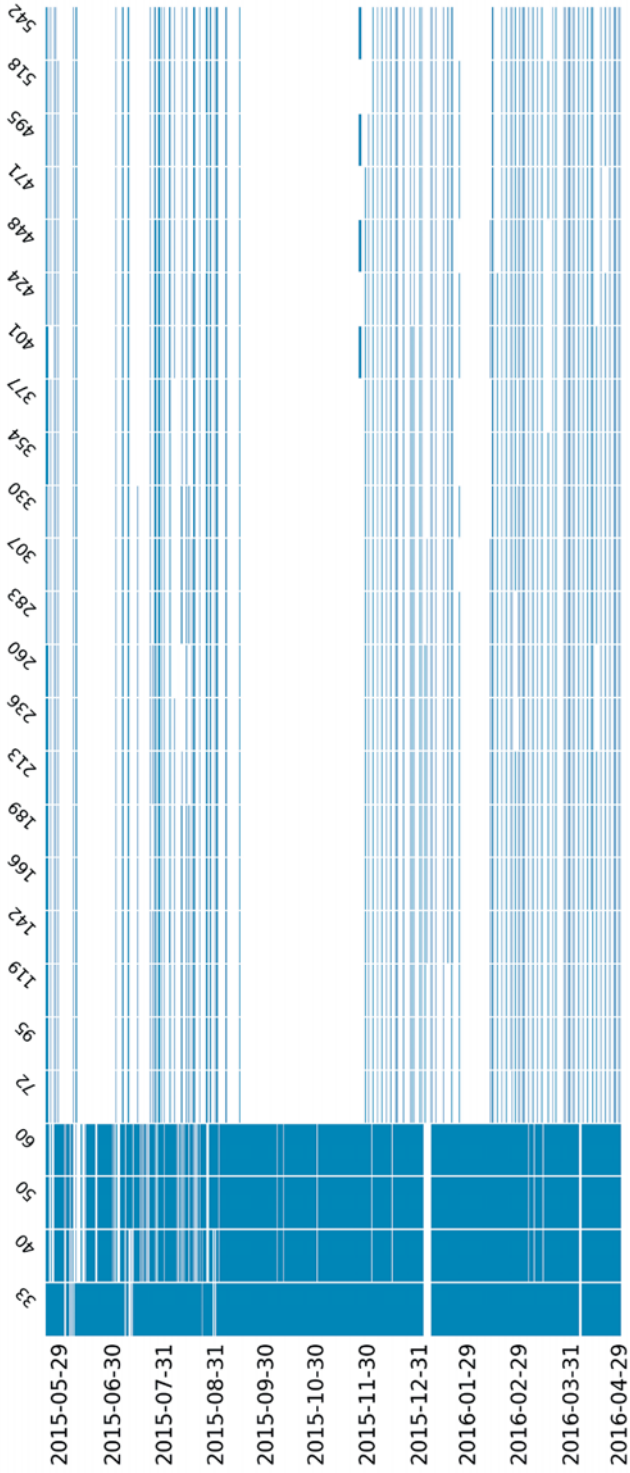

Figure 3: Cup anemometer (33–60 m) and LiDAR (72 m–542 m) data availability of 10 min averages for the whole measuring campaign.

represents a distance of 12 m. After LiDAR and cup anemometer had been combined, the data was averaged to 20 min to avoid misdetection due to long-lasting eddies. Averaging over more than 20 min was not possible, as the raw data sometimes included only 20 minutes of continuous records. The averaging time window for the 20 min averages based on the 10 min averages was not fixed. For instance, some LiDAR recordings were conducted from 00:00:00 to 00:19:59 (resultant time stamps 00:00:00 and 00:10:00) where directly before and after this time-span was at least one NaN value per time stamp due to missing or failure records. In this case, the 20 min average resulted in the time stamp 00:00:00. Instead, if there was a continuous recording for instance between 00:50:00 and 01:09:59 (resultant time stamps 00:50:00 and 01:00:00) and no recordings for time stamps occurred close to this period, this period was averaged to the time stamp 01:00:00. A minimum threshold of two 10 min values per time window was the requirement for making a 20 min average, otherwise, the value resulted in NaN. As LLJs typically last for hours (Baas et al., 2009; Nunalee and Basu, 2014), we expect that the 20 min averages are still sufficient to detect all LLJs. After data processing, 3107 data records of 20 min averages, which are distributed over 250 days, were available for further investigations.

2.1.2 Temperature data

For the thermodynamic related properties of LLJs, temperature profiles were obtained by a HATPRO-RG4 temperature and humidity profiler of the Radiometer Physics GmbH. From this device, we used temperature profile retrievals. The temperature data were available from 20 March 2015 to 04 October 2016 with some larger gaps in between.

The neural network of the radiometer was trained with 15 years (2000–2014) of measurements from radiosondes at Sola (Stavanger), Ekofisk and Orland (Trondheim). As we expect to find especially at Sola and Orland lower yearly average air temperatures than at FINO1 as a natural consequence of the higher latitude, a bias of the retrieved temperature profiles is expected. However that bias cannot be quantified. The temperature climate at Ekofisk should match relatively well the climate near FINO1, although even here a slight bias is expected that affects the profile retrieval calculation. More detailed information about the training method can be found in Churnside et al. (1994) and Radiometer Physics (2015). Fligg (2017), who evaluated one year of temperature and humidity profiles obtained from the HATPRO-G4 profiler at FINO1, found an average correlation coefficient of $r^2 = 0.95$ for the temperature profiles with 643 correlation pairs between radiosondes of Norderney and the microwave radiometer at FINO1 up to 3 km height (personal communication). However, r^2 was lowest at lower heights and increased with altitude. Best correlations were found for heights between 500 m and 800 m ($r^2 > 0.97$). However, the correlation was still around $r^2 = 0.95$ at about 150 m–200 m. Uncertainties in temperature profiles at lower heights are therefore expected for radiometer data. Especially high-frequent temperature variations with height are not represented in the radiometer data by sufficient detail. Nevertheless, the evaluation shows sufficient validity for qualitative analyses of case studies. Fligg (2017)

showed that the radiometer was not able to represent elevated inversions, while near-surface inversions were generally represented. As LLJs may also occur during elevated inversions and due to lower correlations below 500 m, we decided to use temperature retrievals only for the two case studies in which only low-level inversions occurred and not for the statistics. Stuve diagrams of Norderney radiosonde data, showed that during both case studies where the radiometer detected inversions, inversions were also detected by the radiosondes (not shown). In microwave radiometer operation mode during the OBLEX-F1 campaign, erroneous temperature measurements were excluded by the radiometer software. The temperature detected with the sensor at the radiometer, which is required for profile retrieval calculation, has been quality checked. Afterwards, 5–6 measurements in 10 min were averaged. The temperatures were furthermore compared with mast-mounted temperature sensors at 30 m (r = 0.97), 50 m (r = 0.96), 70 m (r = 0.99) and 100 m (r = 0.99).

2.2 LLJ Detection

After preprocessing, we applied for the LLJ detection an algorithm similar to Baas et al. (2009). Based on their main criteria, we used the following definition: First, a maximum in the wind profile must occur below a defined height, and this maximum must be at least 2 ms^{-1} (to avoid misdetections during low wind speeds) and 25 % (to avoid misdetections during high wind speeds) larger than the next minimum above (Figure 4a). Second, if no minimum above the maximum is detected, the value in the last (the highest) layer is assumed as minimum (Figure 4b). We used a maximum detection height of 518 m as described in section 2.1, very similar to the 500 m applied by Baas et al. (2009). In order to draw a broader picture of LLJs above the Southern North Sea, we did not apply further filtering, e.g. to exclude large-scale baroclinic induced LLJs or a certain stability as a prerequisite for LLJ detection, as done by Baas et al. (2009). Apart from that the LLJ profile must be existent in the 20 min-time window, there is no minimum time required that a LLJ counts as a LLJ. That means, if one 20-min record matches the above mentioned criteria, this record is defined as LLJ. Furthermore, if at least one time on a day such a record fits these requirements, this day counts as LLJ-day.

2.3 Stability determination and classification

We applied the dimensionless Bulk Richardson number for stability classification

$$R_b = \frac{\frac{g}{T_v}\Delta\theta_v \Delta z}{(\Delta U)^2 + (\Delta V)^2} \qquad (2.1)$$

where T_v is the absolute virtual temperature, $\Delta\theta_v$ is the virtual potential temperature difference of a specific layer of thickness Δz and ΔU and ΔV are the differences

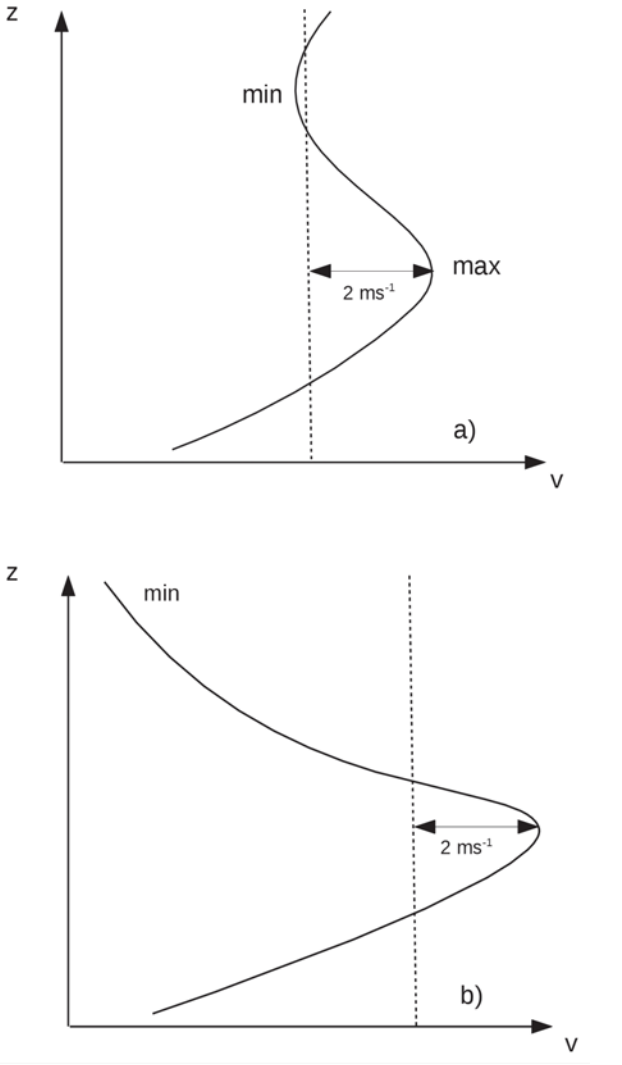

Figure 4: LLJ detection criteria. a) Shows the case if the minimum is below the highest detection level, b) shows the case if the minimum is on the highest detection level.

of the velocity components across that layer. A critical value for R_b is not well defined, although for the gradient Richardson number a critical value is often assumed as R_c = 0.25 where a flow of air is defined as dynamically stable above this value (Stull, 1988). However, contrary to the gradient Richardson number, the value of R_b strongly depends on the shape of the vertical wind profile. If the two measurement points are below and above the LLJ core, R_b is also invalid as it would not represent the vertical wind shear that is actually present in the profile. Thus, Δz should be selected as small as possible. The dependence of R_b on the range of Δz is shown by Dörenkämper et al. (2015a). For the calculation of R_b, we used the data from measurements at 50 and 33 m from the cup anemometers at the FINO1 met mast. For this reason, all LLJs detected with a wind maximum at 33 m height were excluded from the stability evaluation.

In the literature, various thresholds for stability classification on the basis of the Richardson number have

Table 2: WRF setup.

Option	Selection
WRF Version	WRF-ARW 3.8.1 (Skamarock et al., 2008)
Δx, Δy	D1: 27 km, D2: 9 km, D3: 3 km
Pressure Levels	61
Nudging	Analysis (FDDA) Nudging (Stauffer and Seaman, 1994)
Forcing	ERA-Interim (Dee et al., 2011) every 6 h OSTIA (Donlon et al., 2012) every 6 h
Physics	
ABL Scheme	MYNN2 (D1, D2, D3) (Nakanishi and Niino, 2006)
Surface Layer Scheme	MYNN (D1, D2, D3)
Microphysics	Thompson Scheme (D1, D2, D3) (Thompson et al., 2008)
Cumulus Parameterization	Grell 3D Ensemble (D1, D2) (Grell, 1993), (Grell and Devenyi, 2002)
Shortwave/Longwave Scheme	Dudhia (Dudhia, 1989), RRTM (Mlawer et al., 1997) (D1, D2, D3)
Land Surface Scheme	Unified Noah Land Surface Model (D1, D2, D3) (Tewari et al., 2004)

been used (Krogsæter and Reuder, 2015). We used the classification after Lee (2017), where

- $Ri >= 0.25$: strongly stable
- $0.05 <= Ri < 0.25$: stable
- $-0.05 <= Ri < 0.05$: neutral
- $-10 <= Ri < -0.05$: unstable
- $Ri < -10$: strongly unstable.

2.4 Model setup

We used the mesoscale atmospheric model WRF-ARW V3.8.1 (Skamarock et al., 2008) with the Mellor-Yamada Nakanishi-Niino Level 2.5 (MYNN2) (Nakanishi and Niino, 2006) planetary boundary layer (PBL) scheme (Table 2). This scheme was found to capture offshore LLJs at least qualitatively and was not clearly outperformed by others, although it is well known that all schemes have problems to represent the wind shear and jet core speed (Nunalee and Basu, 2013; Nunalee and Basu, 2014; Svensson et al., 2016; Yang et al., 2016). The model was set up with three nested domains of 27 km, 9 km and 3 km horizontal resolution, as shown in Figure 5. The innermost domain covered the Southern North Sea and parts of Denmark, Northern Germany and the Netherlands. In the vertical direction, we used 61 pressure levels, with increasing resolution towards the ground. 22 pressure levels were located within the lowest kilometre. The pressure level distance from surface to first pressure level was 2 m and the distance to

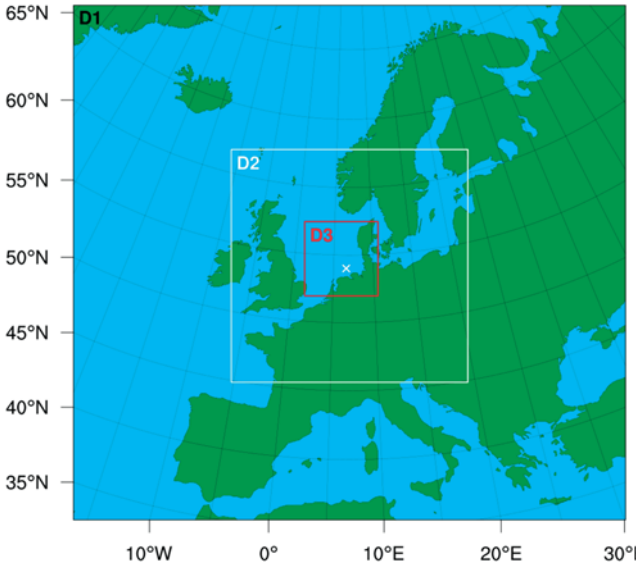

Figure 5: The WRF domain setup. Domain 1 (D1) with $\Delta x, \Delta y$ = 27 km, domain 2 (D2) with $\Delta x, \Delta y$ = 9 km and domain 3 (D3) with $\Delta x, \Delta y$ = 3 km.

the next level above was 16 m, with a continuously increasing spacing to 160 m at 1080 m altitude. Details on the model setup and the chosen parameterizations are shown in Table 2.

WRF runs have been conducted for two case studies, one in August 2015 and one in April 2016, which are introduced in more detail in the next sections. The LLJs were observed at 1420 UTC 13 August–0640 UTC 14 August 2015 (case 1) and 1800 UTC 10 April–0400 11 April 2016 (case 2). We decided to choose a 72 h spin-up prior to the actual model run, as conducted by Dörenkämper et al. (2015b).

The considered periods for model evaluation were finally 0000 UTC 13 August–2300 UTC 14 August 2015 and 0000 UTC 10 April–2300 UTC 11 April 2016. The model outputs, taken at the nearest grid point to FINO1, were interpolated to the observation heights.

3 Results and discussion

LLJ characteristics derived from the 345 days of wind measurements and detailed analyses of two LLJ cases are presented and discussed in the following part. Based on these evaluations of observational- and model data and synoptic situations, possible formation mechanisms are discussed.

3.1 LLJ characteristics derived from long-term measurements

Due to the unavailability of data in several weeks in a row and the limited duration of the campaign (Figure 2, Figure 3), the data is not sufficient for a climatology. Especially the autumn months lack data considerably. Issues are expected for the other time periods, too. For instance, a large lack of data in the summer months might

lead to the potentially wrong conclusion that LLJs occur less often in summer. In the same way, properties of LLJs are affected. The lack of data in summer could lead to the misinterpretation that LLJs occur mainly under westerly wind directions and the average height would be higher. The LLJ detection algorithm does not guarantee that every LLJ profile is a LLJ. Furthermore, the selection of the included parameters for the LLJ definition as well as the determination of the corresponding LLJ thresholds are still individual decisions. In addition, the LLJ frequency is expected to be generally not uniformly distributed over the year as addressed in Section 1. This should be kept in mind for the following analysis and the derived statistical values should be interpreted with care.

LLJs occurred at 14.5 % of the time (449 of 3107 measurements) and on 64.8 % (162 of 250) of the days. Kalverla et al. (2017), who analysed a 4 year data set from the met mast Ijmuiden (Werkhoven and Verhoef, 2012), that is situated to the West of the coast of the Netherlands, found hints for LLJs in the measurements from 12 % of the time for the months of July (here in July 2015: 16.3 %). During all other months, especially during winter, they found considerably lower frequencies. But firstly, they analysed a much longer time series. Secondly, at least part of the discrepancy can be explained by the fact that the maximum observation height in their study was 315 m, while we found LLJs up to our cut-off height of 518 m (Figure 8c). For these reasons, the studies are not well suited for comparisons, although the distance of the Ijmuiden met mast to FINO1 is only about 250 km. Tuononen et al. (2015) presented an 11-year wintertime climatology for LLJs based on reanalyis data in polar and mid-latitude regions of the northern hemisphere, and found a frequency of occurrence of LLJs over the North Atlantic of 5–15 %. However, the comparability is limited as only wintertime was considered and, in addition, a much longer time period was considered. Furthermore, the reanalysis grid resolution was 30 km and, compared to our study, very coarse. Table 3 shows the number of measuring days by month and on how many days LLJs occurred. LLJs in this table are therefore defined as days where at least one measurement on a day was recorded that fits the criteria addressed in Section 2.2. The most LLJ days in our study were found in December 2015/March 2016 (25 days each), January 2016 (24 days) and August 2015/April 2016 (23 days each). However, especially in the winter months December, January and February, several strong-wind events and storms occurred from westerly directions with partially over 30 ms^{-1} wind speed (Figure 7, 10), which could wrongly be interpreted as LLJs. Although all the wind profiles match the LLJ criteria addressed in section 2.2, many profiles within these months show strong vertical variations over small distances, which are not known as typical LLJ wind profiles. In some profiles, the vertical distance between minimum and maximum is only 24 m. An additional stability filtering could be an appropriate solution for LLJ detection. However, as highlighted above, at least by means of a stability estimation with bulk Richardson number, results of relatively high uncertainty are expected.

Table 3: All days by months measured as well as LLJ days during the campaign. LLJs are defined as days where at least one measurement on a day was recorded that fits the criteria addressed in 2.2.

Month	Year	Total Days	LLJ days	LLJ percentage
May	2015	10	2	20 %
June		10	4	40 %
July		31	16	52 %
August		31	23	74 %
September		9	3	33 %
October		10	–	0 %
November		6	3	50 %
December		31	25	81 %
January	2016	30	24	80 %
February		25	13	52 %
March		31	25	81 %
April		30	23	77 %

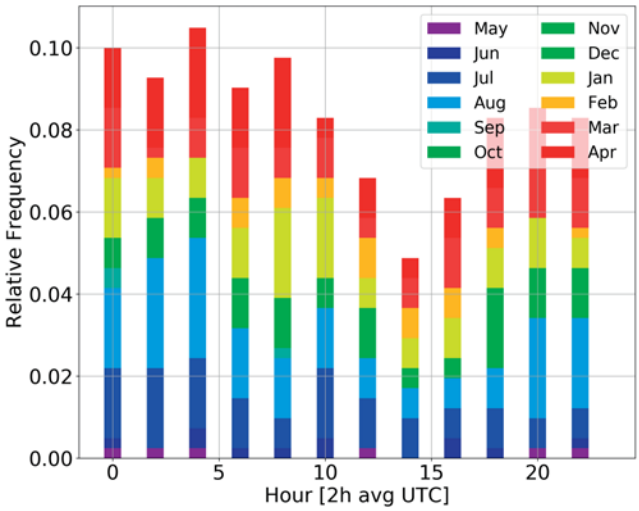

Figure 6: Summarized frequency distribution for LLJ occurrences by hour of the day (bin width = 2 h) and in dependency on months.

Figure 6 shows the distribution of jet occurrences as a function of the time of the day and in dependency on the month. For this evaluation, for each 2-hour interval a value has been derived of the existing 20 min averages, with respect to time-discontinuous measurements in the DBS scan mode as addressed in section 2.1. LLJs occurred mainly during the nighttime hours until noon. Although LLJs were recorded around 1400 UTC, the probability for a jet measurement at that time is only about half of the probability for a jet measurement at 0400 UTC.

The average LLJ speed (the wind speed at jet core height) was 11.8 ms^{-1} with a standard deviation of 5.9 ms^{-1} (median: 10.5 ms^{-1}, min: 2.7 ms^{-1}, max: 46 ms^{-1}). A 15-day moving median shows that the strongest LLJs occurred in the winter months, while the

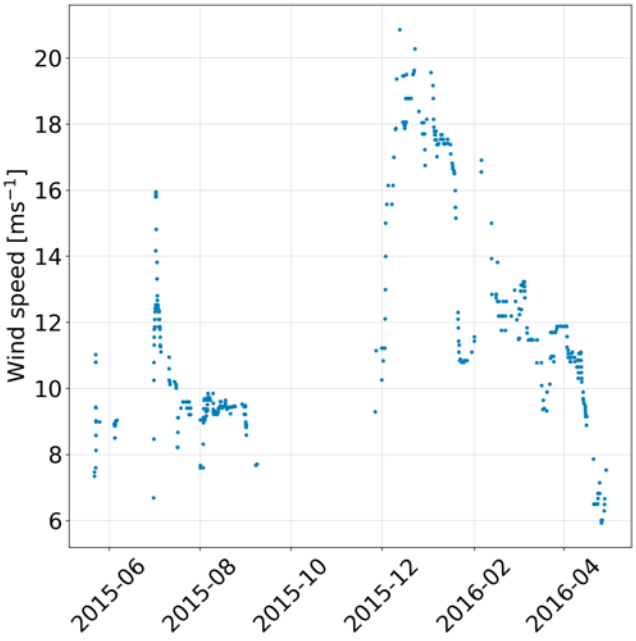

Figure 7: 15-day moving median of LLJ core wind speed over the whole measuring period.

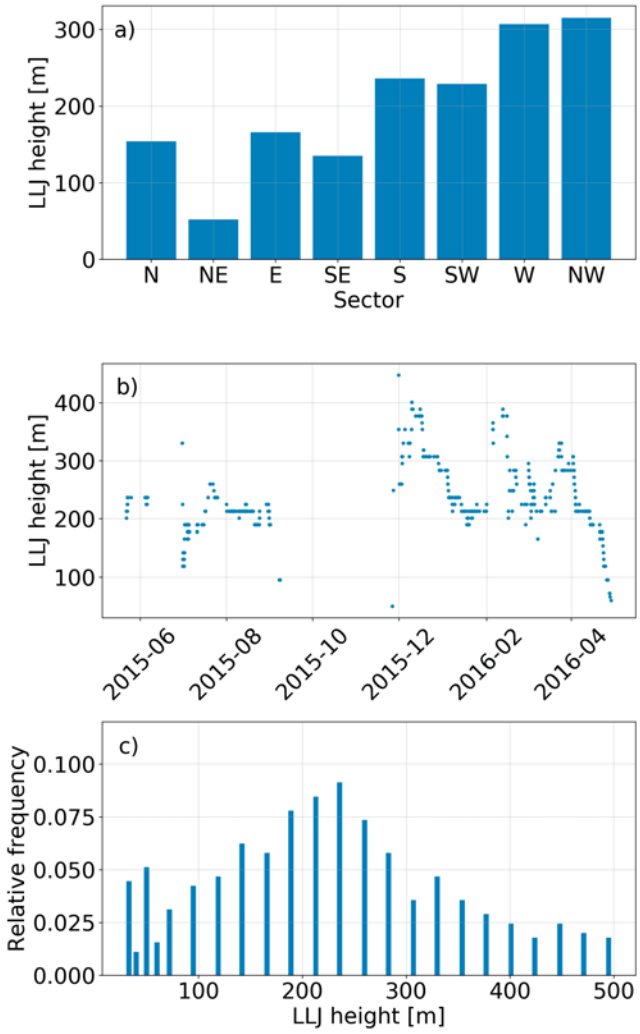

Figure 8: Median LLJ heights for wind direction sectors (a), 15-day moving median of LLJ height over the whole measuring period (b) and frequency distribution for LLJ heights‘(c). The smaller distances between the bars at lower heights in (c) result from the shorter vertical measuring distances between cup anemometers.

wind speed was generally lower during spring and summer (Figure 7). However, as already addressed, the high wind speeds in winter time might simply be a result of westerly storms which are misinterpreted as a LLJ by the detection algorithm.

The highest core heights of LLJs were observed for winds from westerly and northwesterly directions, while the lowest core heights were observed for northeasterly and southeasterly directions (Figure 8a). We observed a seasonal dependency of the LLJ height, with higher levels during the winter months and lower levels during summer and spring (Figure 8b). However, the data availability was especially during the months September, October and November extremely low (Figure 2). Therefore, we generally do not expect a strong evidence of the data for this period.

The frequency distribution of the jet core heights is displayed in Figure 8c. The median of the LLJ core heights that were derived from the measurements was 236 m, and about 9 % of all detected jets occurred at this altitude. The lowest LLJ core heights were observed at 33 m. As this was the lowest measuring level, it remains unclear if the profile that is detected as LLJ due to a wind speed maximum detected at 33 m, is a result of a real LLJ or simply results from negative vertical wind shear.

The results for the height distribution show, that a considerable amount of LLJs occur in the vertical range relevant for newly installed offshore wind turbines. In 2017 these had an average hub height of 96 m and an average rotor diameter of 136 m (Fraunhofer IWES, 2018).

Figure 9 presents the wind roses at 236 m height for all measurements (a) and for the situations with LLJs (b). A comparison between the two wind roses shows, that LLJs are especially likely to occur during easterly to southerly winds. There is also a clustering observed for southeasterly/easterly LLJs during spring and summer and southwesterly/westerly LLJs during the winter months (Figure 10). As LLJs were found to occur at higher altitudes in the winter months, a smaller impact by wind turbine wakes on our LLJ results can be expected for these months. Kalverla et al. (2017) found that the LLJs at Ijmuiden were mostly observed for situations with northeasterly winds, while for FINO1 we could identify South-East as the main direction for the occurrence of LLJs. One reason – besides the limited comparability discussed before – might be that the zone of strongest baroclinicity is more or less parallel to the coastline and aligns the wind direction of the LLJs along the coast of the southern Netherlands more to North-East. However, due to the distance to FINO1, the discrepancy might also origin from synoptic

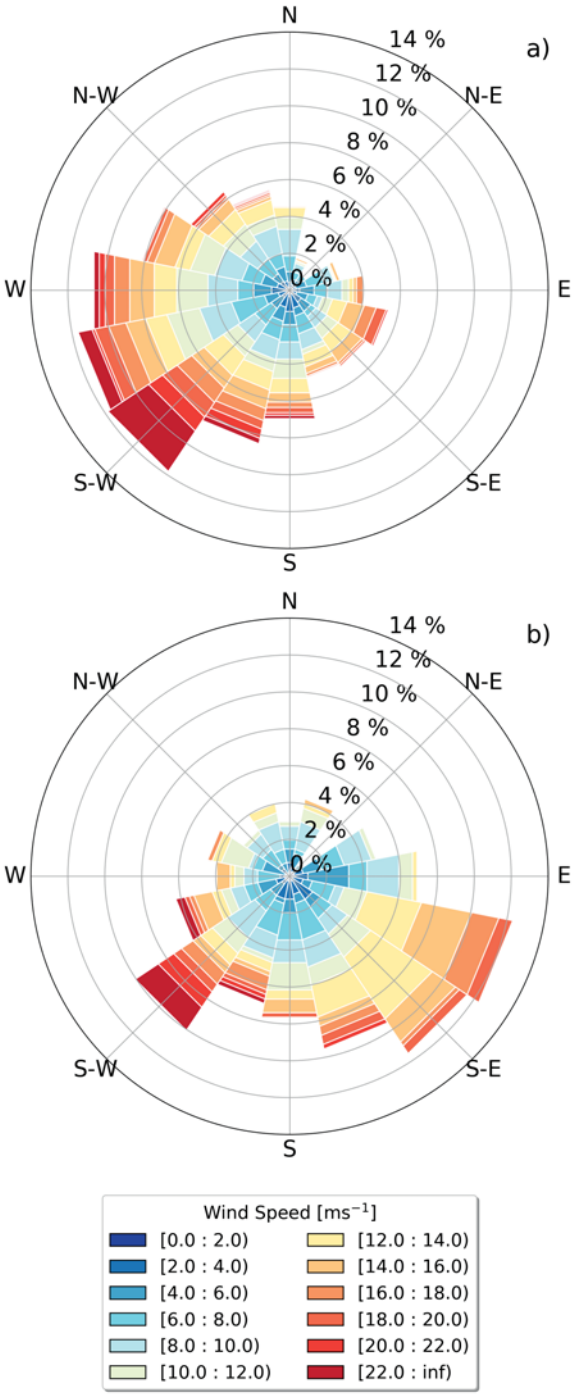

Figure 9: Windrose for all measurements at 236 m height (a) and for LLJ detections at 236 m height (b). Wind speed (colored) is shown in [ms^{-1}] and numbers in the plot show the percentage of wind speed and direction relative to the total amount of (a) all measurements and (b) all LLJ detections.

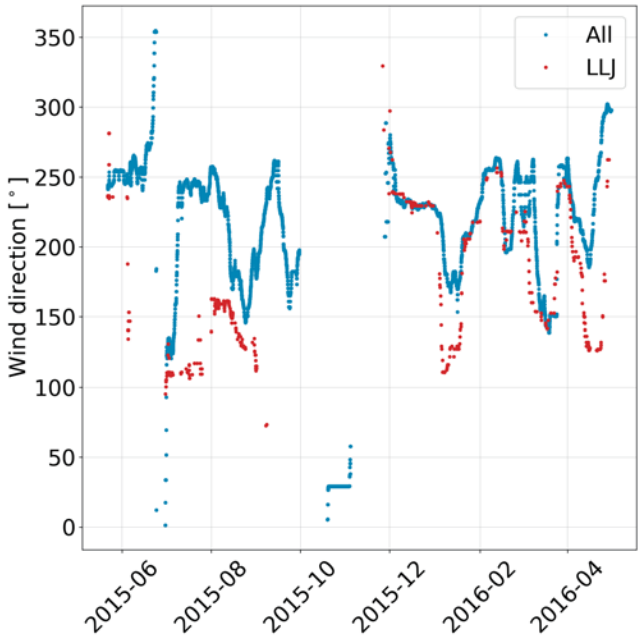

Figure 10: Wind direction over the whole measuring period. The blue dots mark all wind direction measurements at 236 m height while the red dots mark wind directions during LLJ detections at core height.

or mesoscale effects, which differ from the conditions near FINO1. Baas et al. (2009), as well as Floors et al. (2015) observed LLJs mainly from southeasterly directions, although Baas et al. (2009) studied LLJs above Cabauw and Floors et al. (2015) observed LLJs above the north-western coast of Denmark. Dörenkämper et al. (2015b) found the largest number of LLJ events for southeasterly wind directions even above the Baltic Sea. This leads to the question, if there are interconnections between the occurrence of these LLJs and weather patterns. As will be shown later (Section 3.2) we found indeed a merging of a Southern North Sea LLJ with a Baltic Sea LLJ above the Cimbrian Peninsula for one case.

We computed the vertical wind shear of LLJs as

$$shear = \frac{(u_{\max} - u_{33\,\mathrm{m}})}{(z(u_{\max}) - 33\,m)} \tag{3.1}$$

where $u_{\max}$ is the maximum wind speed in the LLJ profile, $u_{33\,\mathrm{m}}$ is the wind speed at 33 m height and $z(u_{\max})$ is the height of the maximum. The evaluation for the shear during LLJs shows, that the highest median wind shear occurred in the sectors North-West and South-East (Figure 11a). However, occurrence of LLJs from North-West is very sparse (Figure 9b), evidence for this statement is therefore limited. No clear dependency on the time of the year could be observed (15-day moving median in Figure 11b), although a peak occurred in July 2015 which is the result of an exceptional difference of wind speeds detected by the cup anemometers and the LiDAR. The reason for this strong difference could not be clarified. The wind shear and wind speed of LLJs correlated only weakly (Figure 11c, $r = 0.27$).

LLJs were evaluated for stability by means of the bulk Richardson number, classified as proposed in Section 2.3. The highest amount of LLJs occurred during neutral boundary layer conditions, followed by highest amounts of stable to very stable conditions (Figure 12a). LLJs during unstable conditions occurred very rarely.

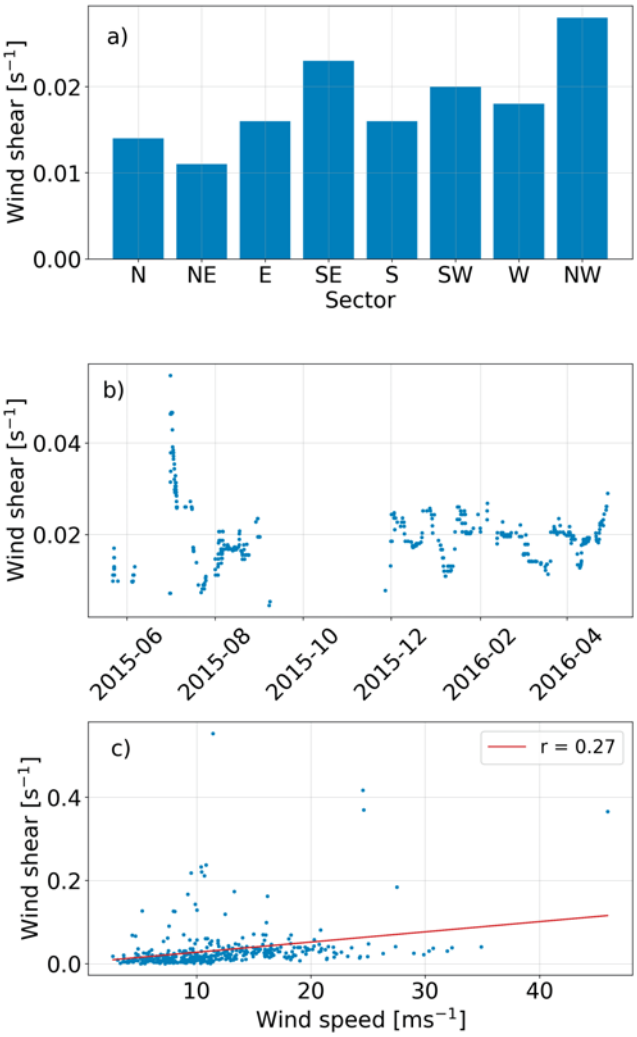

Figure 11: Wind shears during LLJs for wind direction sectors, measured between core height and 33 m (a), wind shear 15-day moving median over the whole measuring period (b) and scatter plot of wind shear and wind speed with regression line (c).

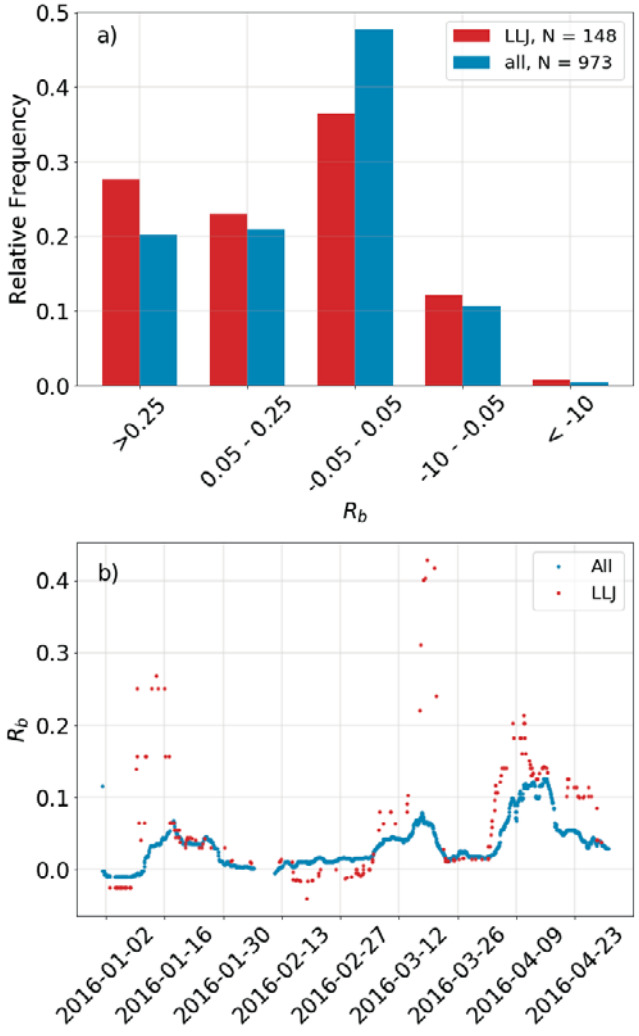

Figure 12: Boundary layer stability for LLJs and all measurements with the bulk Richardson number for 5 stability classes (a). The values have been determined with data obtained from 50 m and 33 m height. Red bars: LLJ cases, blue bars: all measurements. Figure (b) shows the temporal distributions of the 15-day moving median of the bulk Richardson number.

Note, that due to a lack of humidity data during parts of the measuring period only the months January to April 2016 could be evaluated. Furthermore, some situations during westerly winter storms might be misinterpreted as LLJ by the detection algorithm as discussed above. The 15-day moving median stability during LLJs was, in particular during January 2016, considerably higher than during all measurements (Figure 12b). However, the assumption that LLJs mainly occur above stable to very stable ABLs, is possibly valid for LLJs that occur over land at night or offshore LLJs which exclusively originate from frictional decoupling at the coastline (e.g. Smedman et al. (1993) and Dörenkämper et al. (2015b)). Furthermore, the outcome strongly depends on the vertical distance over which R_b is calculated. Our case studies will, indeed, suggest (Section 3.2 and Section 3.3) that at greater heights, in zones where the isentropes are densest, the stability of the ABL during LLJs must be naturally very high. It must also be noted, that FINO1 is located already about 45 km offshore. Under the assumption that LLJs are advected from land over a sea surface – which is the case for LLJs from South-East – our results match the findings of Smedman et al. (1997a) as they state that the stratification close to the shoreline is very stable but becomes almost neutral after a certain advection distance. Mahrt et al. (2014) also found an LLJ under a weakly stable regime. The LLJ was observed on a measuring site about 100 km off the coast, while moderately and very stable regimes during LLJs were found at another measuring site closer to the coast.

3.2 Case 1: 13–14 August 2015

In the following, we investigate an LLJ event that occurred on 13–14 August 2015. We selected this LLJ case, as it featured a distinct jet profile and was well covered by the measurements. We present evidence that indicates three different formation mechanisms of LLJs

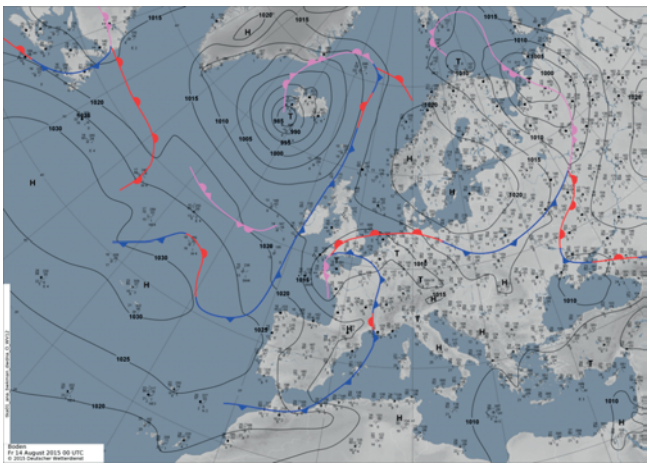

Figure 13: Surface pressure analysis chart for 0000 UTC 14 August 2015 (Deutscher Wetterdienst, 2015).

were involved. Note that we were not able to separate the mechanisms. Nevertheless, we will discuss the different mechanisms in the following:

a) Frictional decoupling

b) Baroclinicity due to land-sea-surface temperature differences and

c) Baroclinicity due to a warm front passage

We will explain our assumptions for the mechanisms by means of observation and model data.

3.2.1 Synoptic situation

The synoptic situation was characterized by a well developed low pressure system with its center just South-West of Iceland and an anticyclone over Scandinavia. South of these two main systems, a weak low was situated above the Netherlands, Belgium and Northern France (Figure 13). The corresponding warm front passed the coastline of North Western Germany northwards. The overall synoptic situation led to a southeasterly geostrophic flow at FINO1. Analyses of satellite images show that most of Germany experienced a nearly cloudless fair weather day. This indicates strong surface heating and an evolution of a deep ABL during daytime over land, followed by a clear night with strong radiative cooling. The geostrophic wind speed at FINO1 was estimated as 14–17 ms^{-1} from the spacing of the isobars.

The weather pattern corresponds to the findings of Baas et al. (2010) and Van De Wiel et al. (2010), who found the existence of an anticyclone above Scandinavia as a favourable weather pattern for LLJ formation at Cabauw. Emeis (2014) studied LLJs above Northern Germany and found the highest likelihood for an LLJ occurrence for a weather pattern including an anticyclone above Scandinavia, as well.

3.2.2 Characteristics

The first detection of the LLJ with the LiDAR was 1420 UTC 13 August 2015 (Figure 14a). At 2140 UTC on the same day, it reached its highest intensity with a wind speed of about 19 ms^{-1}. The last detection of the jet was at 0840 UTC 14 August. The wind speed drop around 100 m height in the early morning might originate from wake effects caused by the wind farm Alpha Ventus situated east of FINO1. The corresponding wind direction profiles (Figure 14b) fit this assumption. The wind shear was about 0.07 s^{-1} at the time of the strongest intensity, measured between 283 m and 119 m height. In the beginning of the jet, the wind direction was mainly East, nearly parallel to the coastline, and turned to South-East during the night. The wind veered strongly at its beginning, from North-East near the ground to a southeasterly direction in upper layers. A nearly linear wind veering was observed around the time of highest LLJ intensity at 2140 UTC. At 0520 UTC 14 August, the wind direction change was about 16°/100 m up to 471 m while the backing above was about −11°/100 m. The veering below the jet core could have been induced by warm air advection while the backing above the jet core could have been generated by cold air advection. This hypothesis is supported by findings of Song et al. (2005). They observed LLJs above the Great Plains with wind veers of 30–50° km^{-1}. Here we found even stronger wind veers. Song et al. (2005) assumed warm air advection as reason for the veering and excluded the Ekman spiral because of low friction in stable boundary layers. Hoxit (1974) and Joffre (1982) also found strong thermal wind effects on wind veer within the ABL. Floors et al. (2015) showed furthermore strong baroclinic influences on the ABL.

The case was represented in the WRF model (Figure 17), although wind shears as well as LLJ intensity were underestimated. This issue was also often addressed in previous studies (Nunalee and Basu, 2013; Nunalee and Basu, 2014; Svensson et al., 2016; Yang et al., 2016). By application of the LLJ criteria, a LLJ was detected from the night before until 13 August 0840 UTC in the LiDAR profile. The next LLJ was detected from 13 August at 1420 UTC until 14 August 1120 UTC (Figure 17a). In WRF, in contrast (Figure 17b), there was no pause detected between the LLJ from 12 to 13 August and the LLJ from 13 to 14 August 2015. Furthermore, the LLJ persisted longer. However, it is expected that the pause that was detected in the LiDAR profiles is a consequence of the missing data at higher levels until around 1400 UTC on 13 August.

A distinct temperature inversion occurred during the jet due to warm air advection, detected by the passive microwave radiometer (Figure 14c). The strongest vertical temperature gradient occurred at 0640 UTC with a maximum temperature of about 293 K at 545 m and a minimum temperature of 290 K at 25 m. The jet core was generally located well below the inversion maximum, i.e. at 0640 UTC at 166 m height. However, as ad-

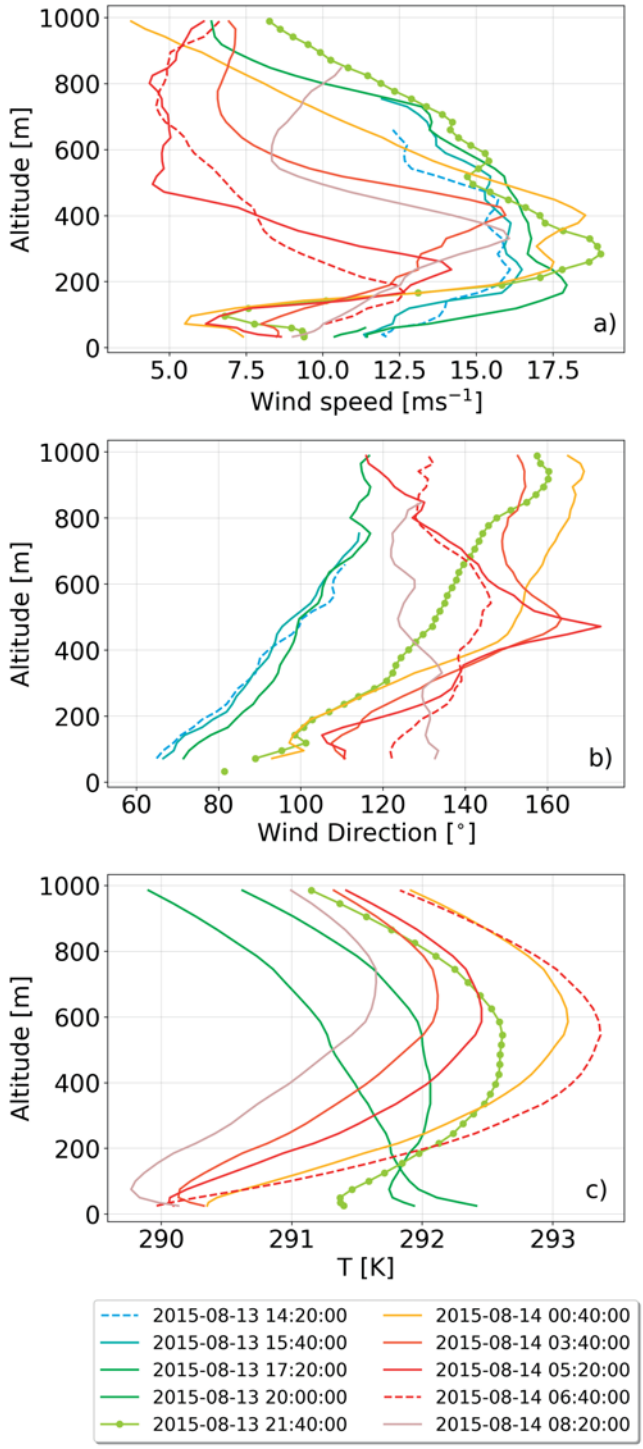

Figure 14: Profiles detected with LiDAR for the LLJ from 1420 UTC 13 August 2015–0640 UTC 14 August 2015 with wind speed (a), wind direction (b) and temperature profiles detected with the radiometer for the same period (c). The dashed lines mark the points of first and last detection of the LLJ and dotted lines mark the point of highest intensity of the jet.

dressed in Section 2.1.2, the temperature profiles of the radiometer are retrievals and not actual measurements over the whole profile like conducted by the LiDAR. Although the device output provided a vertical resolution of 25 m, a vertically highly precise temperature representation is doubted, even if the radiometer temperature profile evaluation showed high correlations. Nevertheless, the modelled potential temperature agreed well with potential temperature profiles retrieved by the radiometer (not shown here).

From the model results one can also see a sloped inversion on the meso-scale, mainly between 0800 UTC and 0200 UTC 13 August (Figure 15 referred to cross section 1 in Figure 1), with much higher potential temperatures above land than over sea at comparable heights. However, the inversion itself appeared to be much more distinctive although less sloped after 2000 UTC until at least to the next morning at 0800 UTC.

Over the whole horizontal distance of the WRF domain D3, the jet was associated with warm air advection and highest wind speeds at the points of strongest vertical potential temperature gradients. Once the zone of strong vertical potential temperature gradients has collapsed (Figure 16f referred to cross section 2 in Figure 1), the jet vanished. Further east, and outside of D3 of the WRF output, the jet extended over a larger area (not shown). It is worth mentioning that the Southern North Sea LLJ indeed merged here with an LLJ coming from the Baltic Sea, flowing from East to West above the Cimbrian Peninsula. This suggests, that LLJs may also extend further westwards and that interactions may occur widely in Northern Europe.

An inertial oscillation was observed from 0840 UTC 13 August to 0040 UTC 14 August, measured at 213 m height, matching well with the theoretical inertial period at FINO1 of $T = 14.8$ h (Figure 18). The inertial period is determined by

$$T = \frac{2\pi}{f} \tag{3.2}$$

where f is the coriolis parameter at a specific latitude. We used 213 m as measuring height for the IO detection as the jet core height was mainly slightly above this height level and the strongest wind vector turning was expected to occur around the jet core height. The cycle shows an elliptical shape typical for the IO, although the cycle is not closed.

3.2.3 Mechanisms

In the following we propose explanations for the formation mechanisms of the LLJ. Vertical cross sections of the model output will give a better understanding of the spatiotemporal evolution of the jet (Figure 1).

We made overlay plots of wind speed and potential temperature along the cross section to investigate the interconnection of wind speed and temperature contrasts between land and sea (Figure 15, 16).

a) Frictional decoupling

The first detection of the LLJ was at 1420 UTC 13 August (Figure 14). In Figure 15, the cross section along

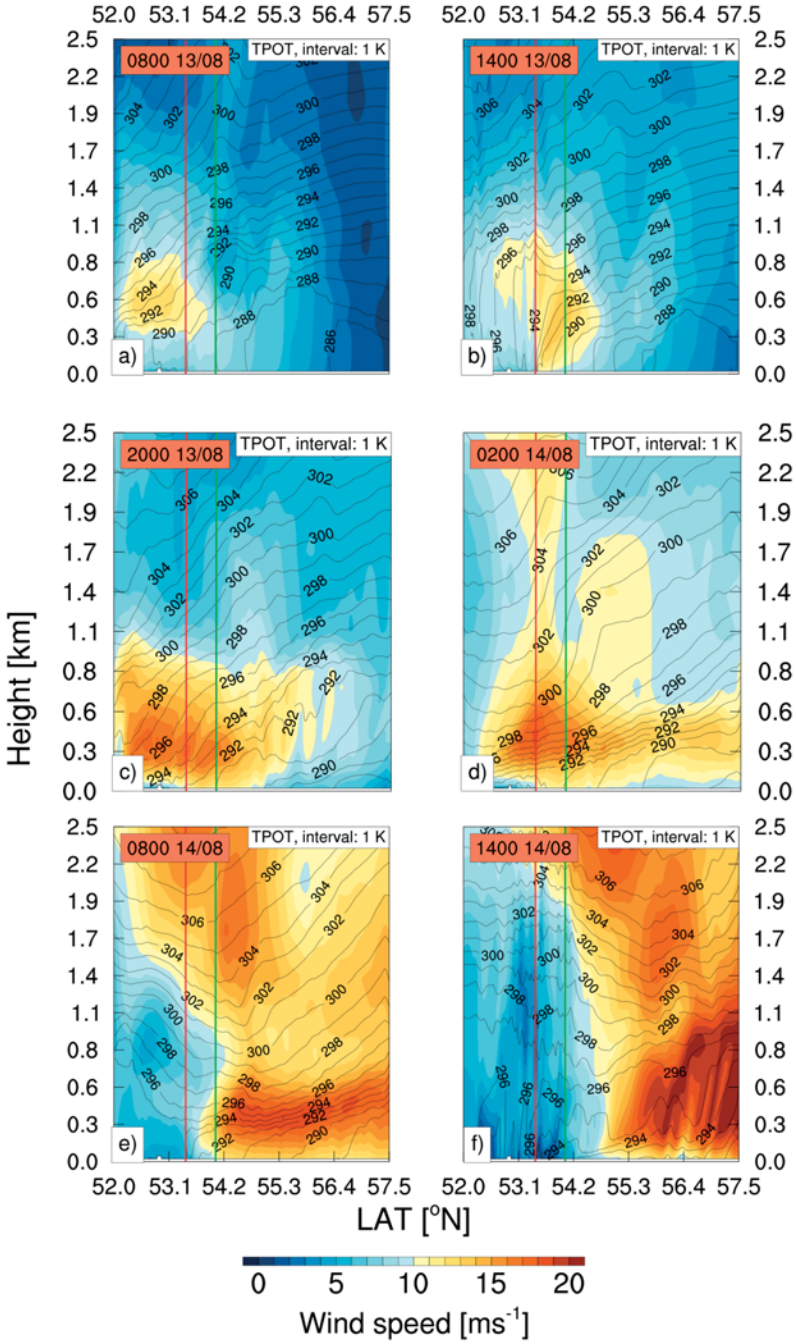

Figure 15: Overlay plot of wind speed (colored) and potential temperature (contour lines) evolution from LLJ 13/14 August 2015 at WRF cross section (1) shown in Figure 1, along the longitude of FINO1. The red line refers to the coastline position while the green line refers to the FINO1 position.

the longitude of FINO1 (section 1 in Figure 1) is shown. At 0800 UTC 13 August, an LLJ already occurred over land at higher altitudes, which evolved the night before (Figure 15). However, a strong baroclinic zone (the area, where the isentropes are densest) evolved at the coastline due to daytime solar heating, with a peak between 1200 and 1400 UTC (Figure 15b). The wind was coast-parallel at this time (Figure 19), and therefore we exclude the coastline of North-Western Germany and the Netherlands as a region where frictional decoupling could have occurred. At this time, the wind rather followed the coastlines of North-Western Germany and the Northern Netherlands and crossed the isobars. Therefore, it appears that the decoupling mechanism was initiated over the western coastline of the Cimbrian Peninsula. As can be seen from the model results, the wind speed above the Cimbrian Peninsula was considerably lower than over the sea (Figure 19a, Figure 16b) at this time, and the LLJ at 1400 UTC was bounded to the east by the western coastline of the Cimbrian Peninsula. On 13 August, the maximum 2-m temperature near the coast was around 23 °C in the afternoon while the SST was

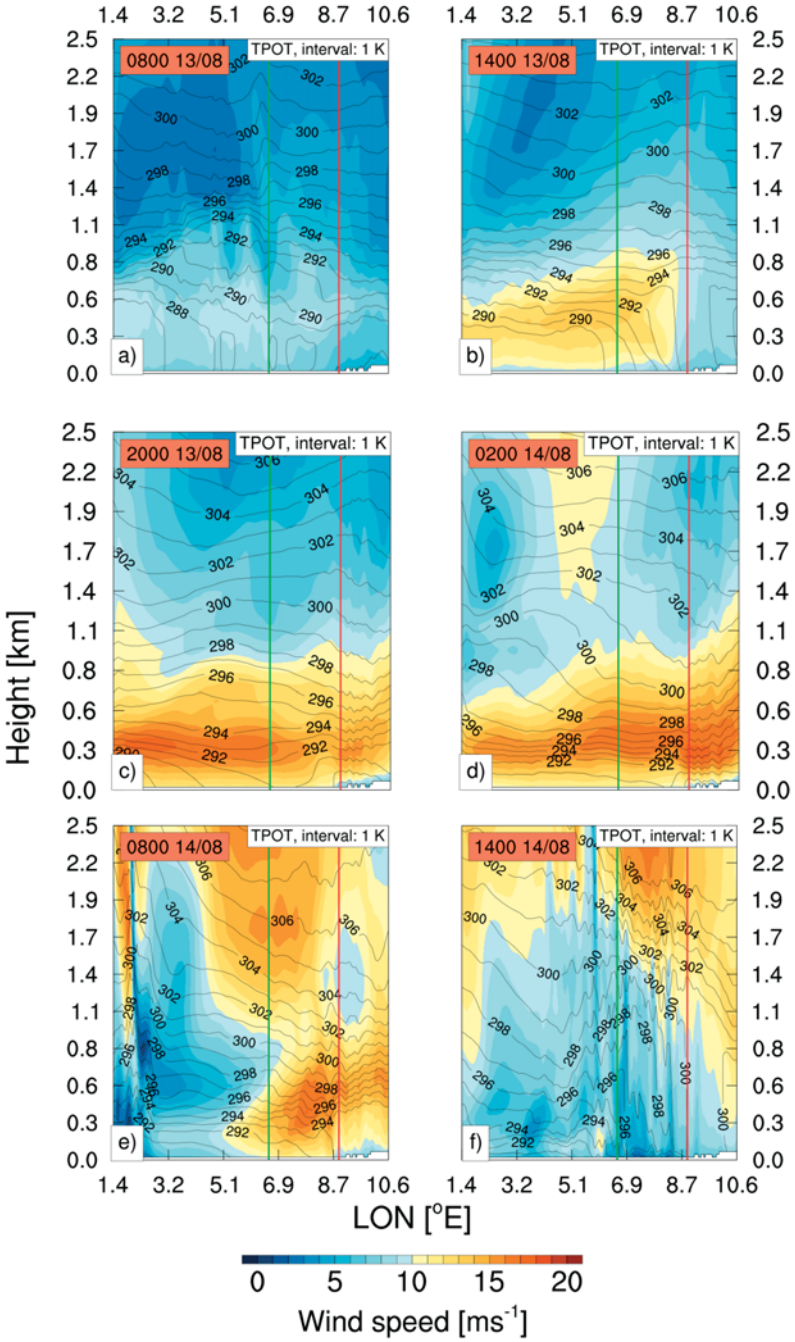

Figure 16: Overlay plot of wind speed (colored) and potential temperature (contour lines) evolution from LLJ 13/14 August 2015 at WRF cross section (2) shown in Figure 1, along the latitude of FINO1. The red line refers to the coastline position while the green line refers to the FINO1 position.

about 18 °C. This indicates generally stable conditions over the sea, as relatively warm air masses from the land are advected over the cooler sea surface. This hints at a frictional decoupling over that coastline at this time.

Considering a later LLJ stadium, Figure 19d (0200 UTC) shows, that the wind had nearly everywhere – even over the land surface – a southeasterly direction, parallel to the isobars. Therefore, the wind over land appeared to be decoupled from the ABL after sunset, as we expect from the momentum equation neglecting frictional effects. At the same time, at about 53° N and 2° E, the wind was directed towards the high pressure which supports the frictional decoupling hypothesis at the coastline of North-Western Germany during a later LLJ stadium. The hypothesized decoupling over the land surface might be a result of the Blackadar mechanism (Blackadar, 1957).

In conclusion, frictional decoupling cannot be neglected for this LLJ case, neither at the western coastline of the Cimbrian Peninsula, nor in a later stadium at the coastline of North-Western Germany and the Northern Netherlands or in a later stadium over the land due

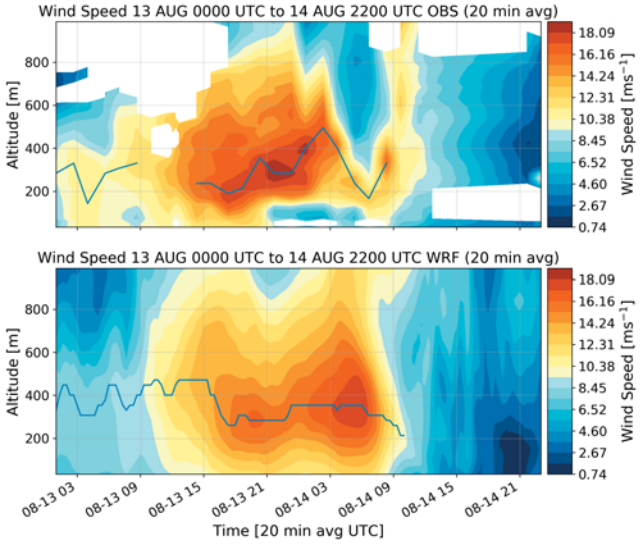

Figure 17: Time-height cross section of the wind speed of the LLJ event 13-14 August 2015, observed by the LiDAR (a) and the corresponding model output of the WRF simulations (b). The blue solid lines show the detected LLJ core height in time dependency. However, it is highly likely that without the missing data at higher levels in the LiDAR data, a LLJ would have been detected for all times in a).

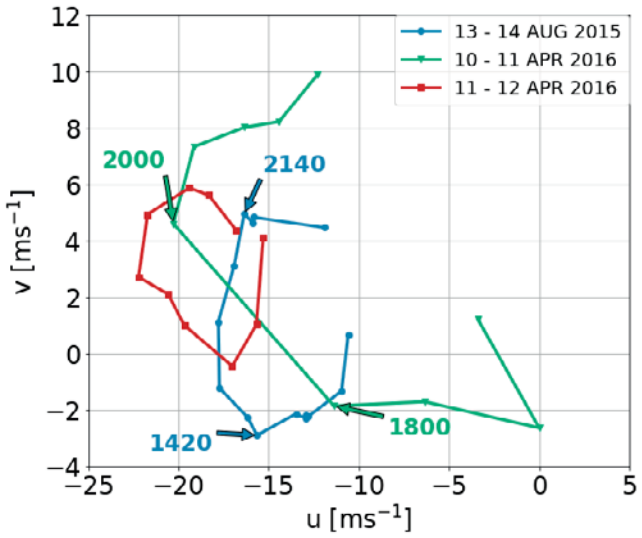

Figure 18: Recorded inertial oscillations during LLJs on 13–14 August 2015, 10–11 April 2016 and 11–12 April 2016, measured at 213 m height. The numbers show the time (in chronological order), where: (1) the LLJ was initiated, (2) the LLJ had its highest intensity and the wind direction matched the geostrophic wind direction for the first time. The IO on 11–12 April 2016 was simply plotted for demonstration of a nearly fulfilled IO period.

to nocturnal cooling. However, for jet initiation we will describe a potentially more important mechanism in the following.

b) Baroclinicity due to land-sea-surface temperature differences

We will concentrate here on the analytical view of mesoscale, thermal impacts on the jet formation. For the observed LLJ, 1200 to 1400 UTC was identified as time of strongest baroclinicity in the coastal zone (Figure 15b), which was caused by the relatively warm air column above land and the cooler air column above the sea. Therefore, we begin to investigate the WRF output at this time. Contrary to mechanism a), we will apply an analytical way that will yield a higher validity for this assumption.

For including baroclinic effects we apply the thermal wind relation (e.g. Martin (2006)), integrated from lower pressure level p_1 to upper pressure level p_2 and under the assumption of a hydrostatic, stationary and geostrophic flow (under neglection of friction). We can then approximate the thermal wind components as

$$u_T = u_2 - u_1 = -\frac{R}{f}\frac{\Delta\overline{T}}{\Delta y}\ln\left(\frac{p_1}{p_2}\right) \tag{3.3}$$

$$v_T = v_2 - u_1 = \frac{R}{f}\frac{\Delta\overline{T}}{\Delta x}\ln\left(\frac{p_1}{p_2}\right) \tag{3.4}$$

where $R = 287.058\,\mathrm{J\,kg^{-1}\,K^{-1}}$ is the specific gas constant for dry air and $\overline{T}$ is the vertically averaged temperature of a layer between two pressure surfaces p_2 and p_1. We found from the model results at 1400 UTC 13 August (Figure 15) a South-North temperature gradient of $\frac{\Delta\overline{T}}{\Delta y} = -1.7\cdot10^{-4}\,\mathrm{K\,m^{-1}}$, which was measured along cross section (1) (visualized in Figure 1) at 300 m height and over a distance of 15 km with its line center point at the model grid point horizontally nearest to the coastline. According to our model results the temperature gradient along cross section (1) (Figure 1) from south to north was about $\frac{\Delta\overline{T}}{\Delta y} = -1.7\cdot10^{-4}\,\mathrm{K\,m^{-1}}$ at 300 m over a distance of 15 km with its line center point at the model grid point horizontally closest to the coastline at 1400 UTC 13 August (Figure 15). Selecting $p_1 = 980$ hPa and $p_2 = 920$ hPa (corresponding to about 300 m and 800 m height, respectively). Eq. (3.3) yields a thermal wind of $u_T \approx 26\,\mathrm{ms^{-1}}$ between these two heights. The wind speed itself is determined by the high-pressure system in its north and the low pressure system in its south (Figure 13, Figure 19). From about 300 m upwards however, the thermal wind $\vec{V}_T$ explains the wind speed reduction and also most likely the wind veer. Thus, the jet shape may be explained by frictional drag close to the ground (e.g. Beardsley et al., 1987; Soares et al., 2014) and the thermal wind in upper layers. We did not observe such a pronounced jet as expected from the thermal wind relation at the time of LLJ initiation at about 1200–1400 UTC. For an explanation of this time shift of about 5 hours between strongest baroclinicity and strongest LLJ intensity, we point to the study of Burk and Thompson (1996) and link to the observed IO (Figure 18). Burk and Thomp-

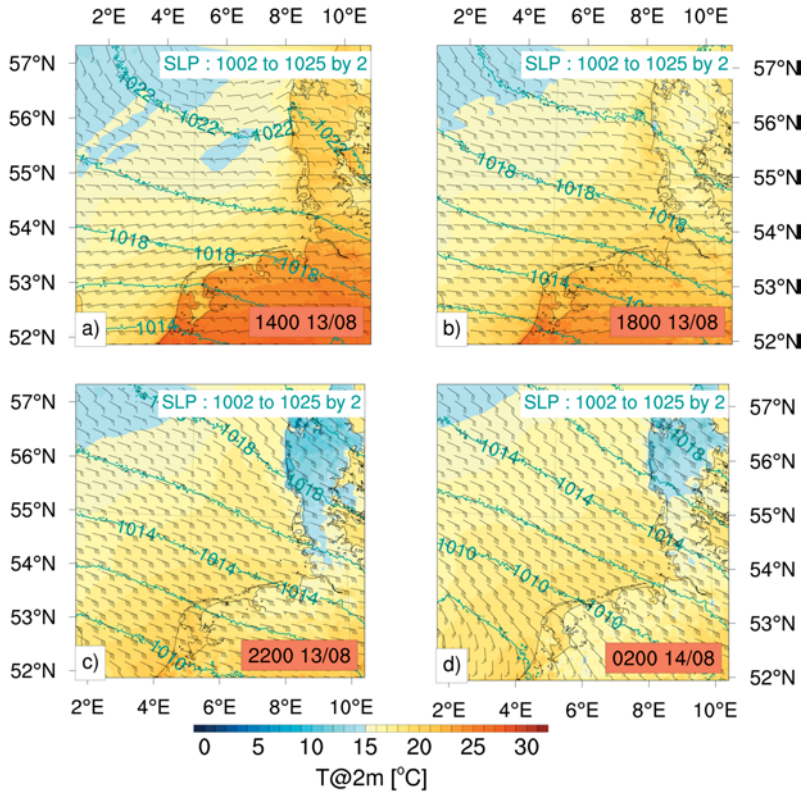

Figure 19: Model results showing the evolution of horizontal distributions of wind speed and direction at 990 hPa (wind barbs), temperature at 2 m (colored) and surface pressure (contour lines) at (a) 1400 UTC 13 August, (b) 1800 UTC 13 August, (c) 2200 UTC 13 August and (d) 0200 UTC 14 August 2015.

son (1996) investigated the summertime LLJ along the Californian coast and found that baroclinicity due to differential surface heating between land and sea mainly shaped the LLJ profile and formed the important environment for the formation and persistence of the LLJ. They observed – as we did – the LLJ maximum 5 hours after the time of strongest baroclinicity and explain the IO as a result of diurnal ABL variations over land, derived from a sea breeze dynamics approach after Haurwitz (1947). They could show that the IO's elliptic phase was set when the wind vector was most aligned onshore and that the orientation and shape of the ellipse determined the time of the LLJ maximum.

Here, we found a maximum of the LLJ when the wind direction during the IO matched the geostrophic wind direction (2140 UTC) and a setting of the IO phase when the wind direction was most onshore (1420 UTC) within the IO cycle. Although an LLJ from the previous night was still existent at 0800 UTC (Figure 15a) – the modelled LLJ initiation on 13 August at the coastline was around 1200–1400 UTC (Figure 15b), during the existence of a strong baroclinic zone and when the wind vector was aligned most onshore. At this point, the IO phase was set. At around 2140 UTC, we found the observed LLJ maximum wind speed with a direction of about 106°, which matched indeed roughly the geostrophic wind direction (model at 2200 UTC: 117°). As the time went by, the marine ABL was consequently capped by a sloped inversion, with lower inversion height over land and a higher inversion height over the sea as also found by Burk and Thompson (1996); Colle and Nowak (2010); Helmis et al. (2013) (Figure 15, 16). As the sloped inversion extended far to the North, the LLJ was extended as well more horizontally while it was vertically more narrow than at LLJ initiation at 1420 UTC.

In addition to baroclinicity and inertial oscillations, we found consistent results of wind speed, core altitude and temporal evolution of the LLJ with an idealized model run of Burk and Thompson (1996). In this setting, they adjusted the terrain height to zero and compared it with the results of the control run. They did not find considerably lower wind speeds of the jet, but lower altitudes, a wider extension and a more westerly direction. They found furthermore that the jet peak occurred three hours later (0100 Pacific Standard Time (PST)) than in the control run with terrain heights (2200 PST). Very similar findings for the influence of baroclinicity on LLJ formation have been found by Colle and Nowak (2010), who investigated the New York Bight jet. Helmis et al. (2013) reported also consistent results, from an investigation of the summertime LLJ along the east coast of the U.S.A. based on observation data obtained from a measuring site at Nantucket island, Massachusetts. All studies agree on the importance of a sloped marine ABL inversion due to differential heating over land and water for the LLJ formation near the coast.

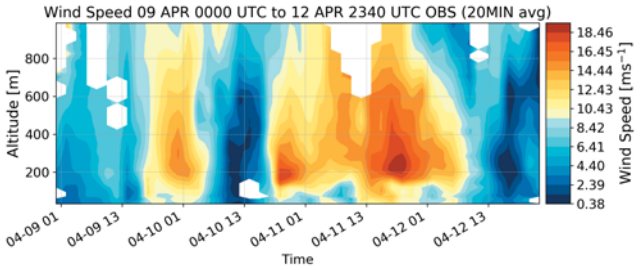

Figure 20: Three Low Level Jets in three nights in a row detected with LiDAR between 0000 UTC 09 April–2300 UTC 12 April 2016 at FINO1.

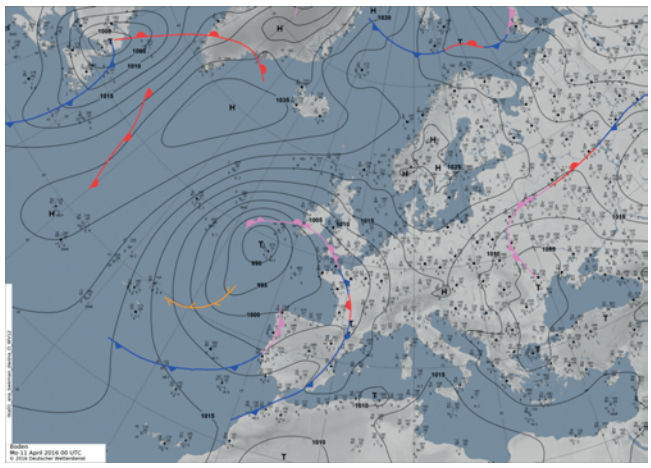

Figure 21: Surface pressure analysis chart for 0000 UTC 11 April 2016 (Deutscher Wetterdienst, 2016).

c) Baroclinicity due to a warm front passage

As addressed in section 3.2.1, a warm front passed the coastline of North-Western Germany between 13/14 August (Figure 13) and reached FINO1 close to the time of highest intensity of the jet (2140 UTC). It was found in the past, that baroclinicity induced by fronts can form LLJs (Song et al., 2005). As shown by Lundquist (2003) and Helmis et al. (2013), fronts can also enhance IOs. This might be a further reason for the high jet core wind speed of about 19 ms^{-1} on 13–14 August.

In summary, our findings show that it seems possible, that LLJs occur at the same time above land, induced by the Blackadar mechanism, and at the coastline due to either frictional decoupling or baroclinicity.

3.3 Case 2: 10–11 April 2016

In the second case, an LLJ has been detected between the evening of the 10 April and the morning of the 11 April 2016. It is noteworthy, that this LLJ came along in a row of three LLJ events during three consecutive nights (09/10 April, 10/11 April, 11/12 April 2016) (Figure 20). A very similar pattern has been observed by Nunalee and Basu (2014). Hence, these jets were characterized by distinct diurnal variations in wind speed. However, only the LLJ of 10/11 April 2016 is investigated in detail in the following. Although some jet characteristics are similar to case 1, differences are noticeable, especially during the formation period. In case 2, an indication for an IO as formation mechanism is much stronger than in case 1, as the wind direction was more southeasterly from its beginning. Furthermore, this LLJ formed shortly after the breakdown of a sea-breeze front. Additionally, no warm front passed FINO1 around the time of LLJ formation. Therefore, we will concentrate on the frictional decoupling mechanism at the coastline.

3.3.1 Synoptic situation

On 10/11 April 2016, a similar synoptic situation occurred as on 13/14 August 2015. The surface pressure analysis chart from 0000 UTC 11 April 2016 in Figure 21 gives an overview of the situation. Again, an anticyclone was situated above Scandinavia. However, an extensive cyclone was situated to the West of the British Isles and, in contrast to case 1, no warm front was in the close proximity of FINO1. Similar to case 1, the isobars indicate a southeasterly geostrophic flow. Above Northern Germany, fair weather conditions were predominant without substantial amounts of clouds, favoring strong surface heating over land during daytime and corresponding strong radiative cooling during the night.

3.3.2 Characteristics

The first detection of this LLJ was on 1800 UTC 10 April 2016 while its last observation was on 0400 UTC 11 April (Figure 22a). The highest wind speed was measured at 2000 UTC with a magnitude of about 18 ms^{-1}. The wind shear at this point was strong with 0.07 s^{-1}, measured between 33 m and the jet core height at 166 m.

The LLJ was represented well by the model (Figure 23). Particularly the altitude of the jet core as well as wind speed and the time of occurrence appear to be modelled properly without a significant time-shift. However, by means of the detection algorithm it shows that the occurred LLJ was only partially detected in the WRF output. The blue solid lines in Figure 23 show LLJ core heights in dependency on time. The wind shear of this LLJ was slightly underestimated.

Considering the LLJ wind direction (Figure 22b), it stands out that at the time of strongest LLJ development at 2000 UTC, the wind direction was very constant with height at about 100°. This is very different to case 1, where the wind veer was strong at each time. However, in case 2, before and after 2000 UTC, the wind veered relatively strong, i.e. 17°/100 m, measured between 50 m and 283 m height at 0400 UTC. Above, the wind backed and the wind direction became very similar to or even more easterly as near to the bottom. It is noteworthy, that at 1200 UTC and 1400 UTC, a couple of hours before the first jet detection, the wind direction differed considerably in height, compared to later hours. The synoptic

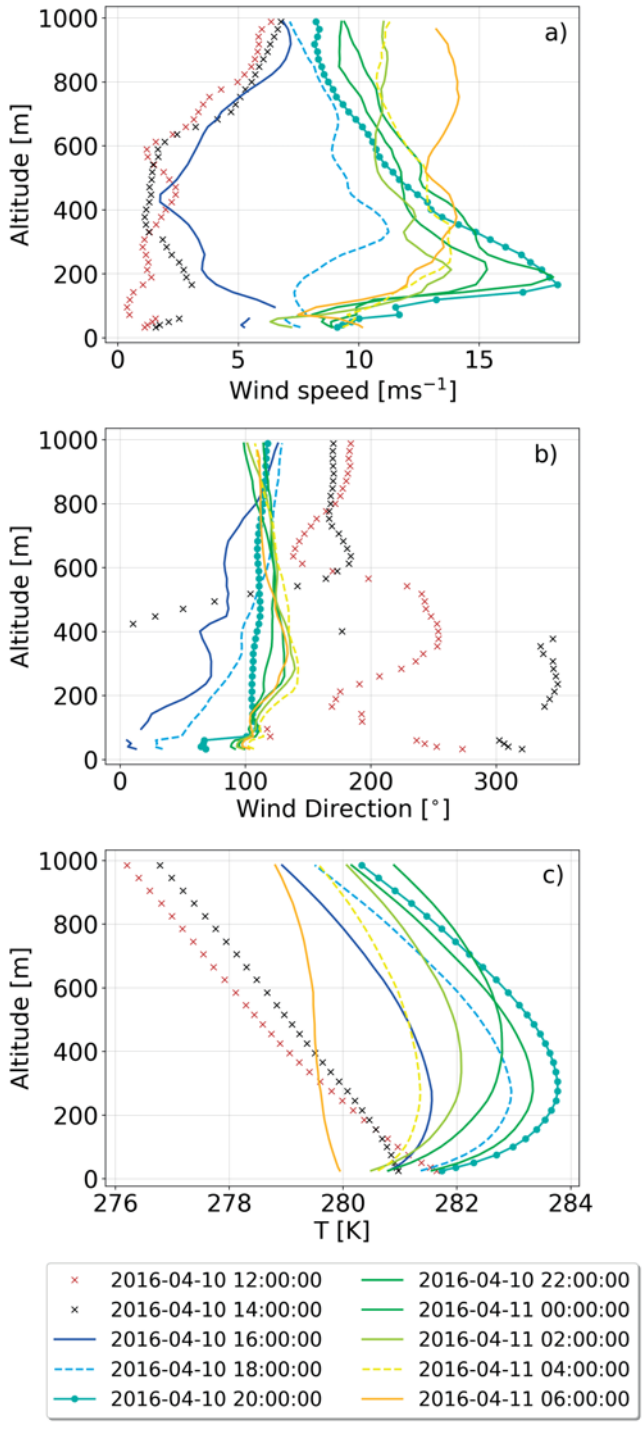

Figure 22: Profiles detected with LiDAR for the LLJ from 1800 UTC 10 April 2016–0400 UTC 11 April 2016 with wind speed (a), wind direction (b) and temperature profiles detected with the radiometer for the same period (c). The dashed lines mark the points of first and last detection of the LLJ and dotted lines mark the point of highest intensity of the jet. The crosses mark the profiles before the jet initation.

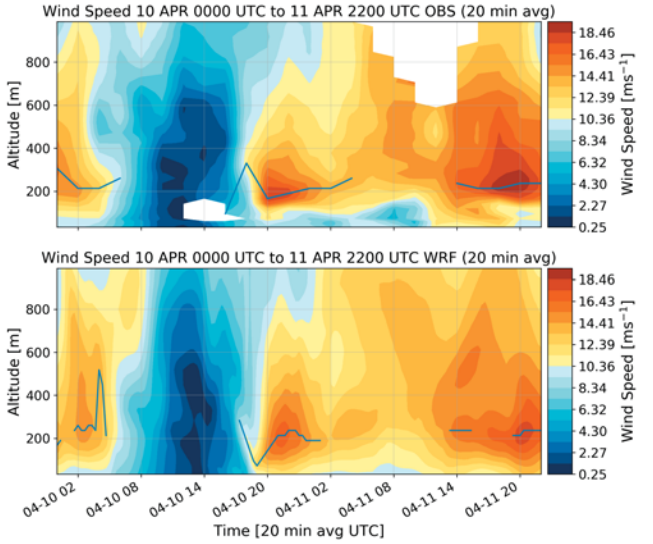

Figure 23: Time-height cross section of the wind speed of the LLJ event 10-11 April 2016, observed by the LiDAR (a) and the corresponding model output of the WRF simulations as 20 min avg (b). The blue solid lines show the detected LLJ core height in time dependency. The higher variations with time in (b) originate from the higher temporal resolution in the WRF output which was originally 10 min instantaneous output averaged to 20 min while the LiDAR had at this time a temporal resolution of 2 h, though 20 min averages were considered for both figures.

situation and the clear sky at 1200 UTC which can be seen from satellite images of that day (not shown), indicate the existence of a see-breeze. Furthermore, DWD station data at Norderney shows for 1230 UTC a wind speed of 3.6 ms^{-1} and a wind direction of 350° while Borkum, for instance, showed at 1100 UTC a onshore wind speed of 3.5 ms^{-1} with a wind direction of 300°. The assumption of a sea-breeze is also supported by the model results (Figure 24a), which show – although calm – onshore wind at 1200 UTC. Cross sections of the WRF output (not shown here) show a slight updraft of 0.3–0.5 ms^{-1} over land between 1200 UTC and 1800 UTC, which might be a symptom of a sea-breeze. Besides, wind direction cross sections of the WRF output show a front from sea level up to above 1000 m directed towards the coastline (not shown here). Nevertheless, the existence of a calm sea breeze is likely, albeit not proven.

Figure 22c shows the temperature profiles during the LLJ. Again, as in case 1, a temperature inversion has been observed, while the temperature maximum e.g. at jet maximum time at 2000 UTC, was located at about 275 m and therefore above the jet core. At 1200 UTC and 1400 UTC, about four to two hours before the first jet detection, no temperature inversion occurred. The inversion during the LLJ event was therefore a result of warm air advection from above the land. Considering the wind direction of about 100–140°, the warm air was transported from the land over the sea along the location of FINO1, which is evident from the visualisation of the model results (Figure 24).

As in case 1, an IO has been observed (Figure 18). The IO plots shown are hodographs based on U and V components recorded at 213 m, similarly to Baas et al. (2012). However, contrary to Baas et al. (2012) we did not apply a normalization by the geostrophic wind. The

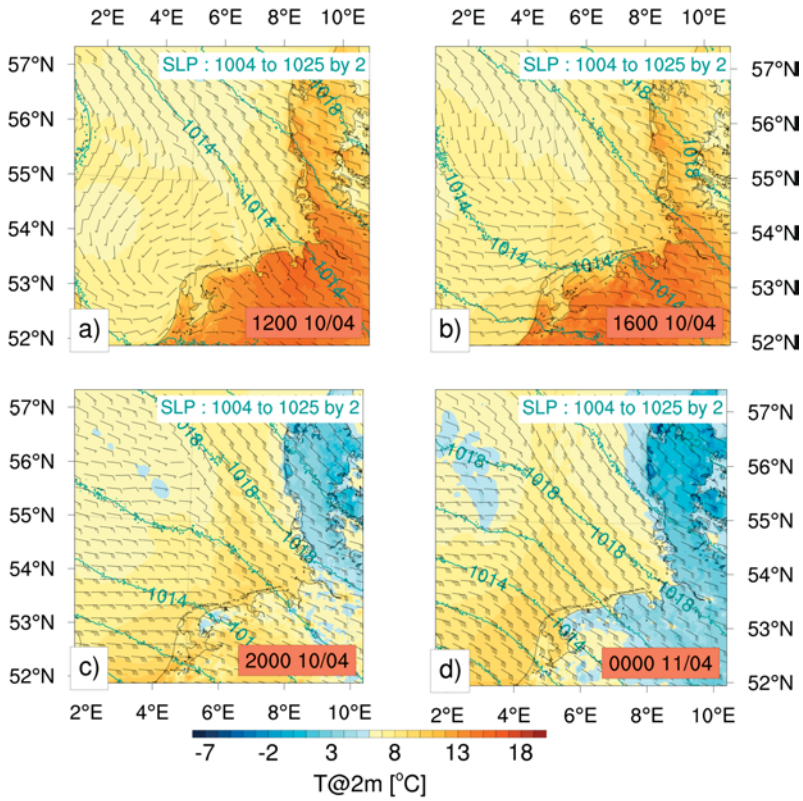

Figure 24: Model results showing the evolution of horizontal distributions of wind speed and direction at 990 hPa (wind barbs), temperature at 2 m (colored) and surface pressure (contour lines) at (a) 1200 UTC 10 April, (b) 1600 UTC 10 April, (c) 2000 UTC 10 April and (d) 0000 UTC 11 April 2016.

IO's initiation was detected as 1200 UTC 10 April, only about four hours before the first jet detection. A stopping of the IO was detected at 0400, which is the time when the LLJ vanished. Thus, the observed IO period of about 16 h matched the theoretical value of 14.8 h again relatively well.

3.3.3 Frictional decoupling after sea-breeze breakdown

As described above, the synoptic situation was very similar to case 1. However, the mesoscale situation before and around the first jet detection was considerably different. It is obvious that at 1200 UTC 10 April (Figure 24a) – about four hours before the first jet detection – the estimated horizontal synoptic pressure gradient near FINO1 was small with about 0.004 hPa km^{-1}. The wind barbs show onshore winds at this time while a large horizontal temperature gradient between land and sea occurred. The SST at 1800 UTC was only 6.8 °C, while the 2-m land temperature near the coast was about 15 °C (both not shown here). For about 1200 UTC, the stability evaluation gave $R_b = -0.13$ which is unstable after the classification of Lee (2017). However, from 1200 UTC, the stability started to increase and reached a maximum at 1800 UTC, with $R_b = 0.98$, thus, strongly stable. Afterwards, the stability declined again.

The wind pattern changed at about 1600 UTC (Figure 24b), two hours before the first jet detection. The wind started to turn to easterly near FINO1. This time, only light winds are evident from the latitudinal cross section (Fig 25b, referred to section 2 in Figure 1) and no wind in the 135° cross section (Figure 26b, referred to section 3 in Figure 1). At 2000 UTC (Figure 24c, 25c, 26c), the wind speed increased considerably and started to turn southeasterly. At this time, the land surface has already cooled down. Four hours later, at 0000 UTC 11 April (Figure 24d), the wind direction was mainly parallel to the isobars and even crossed them to the right. This gives an indication for frictional decoupling.

The IO of the LLJ from 10–11 April could be observed from 1200 UTC to 0400 UTC, with its start about 6 hours before the first jet detection at 1800 UTC (Figure 18). This is similar to case 1, where the IO was existent from 0840 UTC to 0040 UTC. Again, the LLJ was initiated when the wind was directed with its largest angle towards the coastline during the IO cycle. In case 2 we found, contrary to case 1, strong indications for a see breeze circulation which vanished before jet initiation. Similar findings were made by Angevine et al. (2006), where an LLJ evolved over land shortly after a sea-breeze breakdown and headed towards the sea afterwards. Indeed, case 2 came along with a rather South-East wind direction from its beginning, shortly after the potential sea-breeze breakdown (Figure 22b). Furthermore, the jet core altitude was generally lower and the wind shear higher at the time of highest jet intensity,

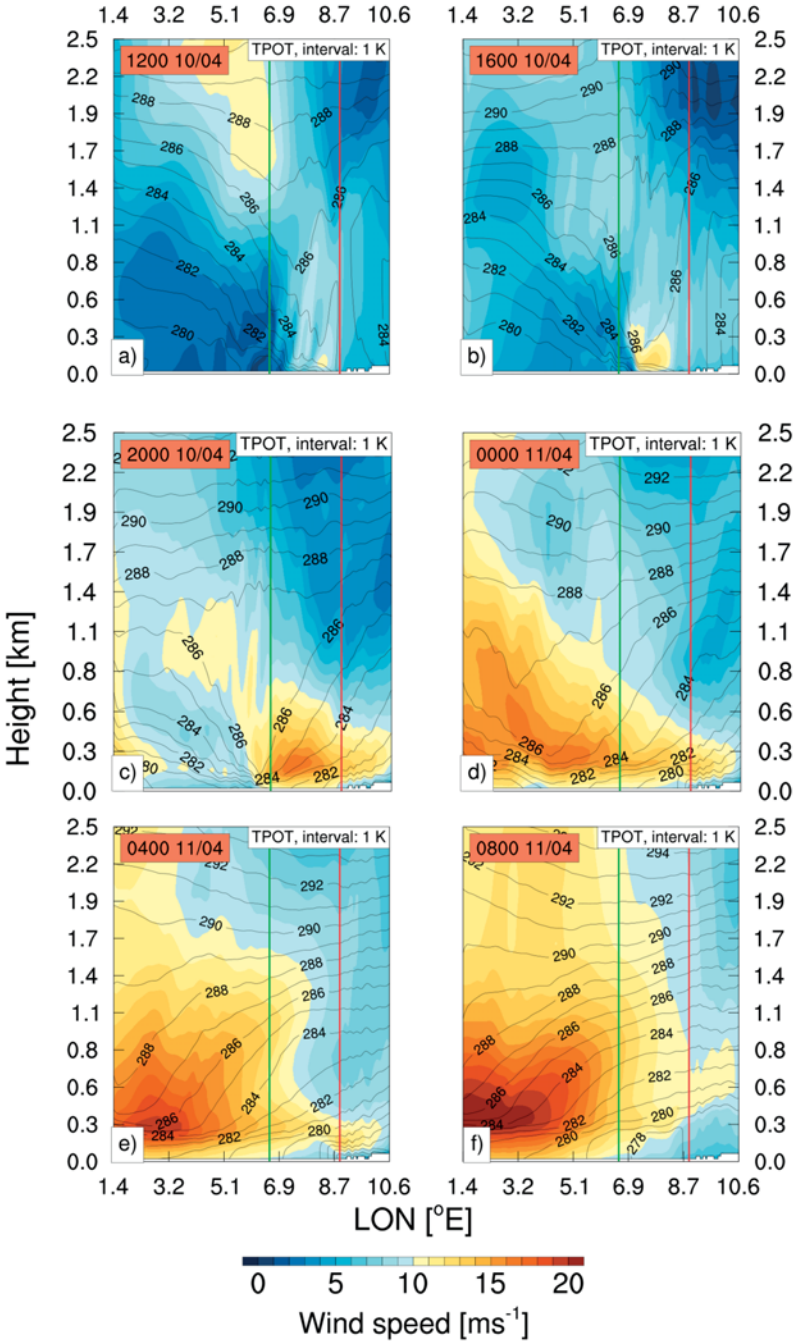

Figure 25: Overlay plot of wind speed (colored) and potential temperature (contour lines) evolution from LLJ 10/11 April 2016 at WRF cross section (2) shown in Figure 1, along the latitude of FINO1. The red line refers to the coastline position while the green line refers to the FINO1 position.

compared to case 1. For case 2, we found a very stable ABL around LLJ formation at 1800 UTC. The large land surface–SST contrast addressed above, might have led to a fast stabilization in the marine ABL when the wind was crossing the coastline from the land towards the sea (Mahrt et al., 2014). As described above, the wind direction was either parallel to the isobars around 0000 UTC or the wind was directed even slightly towards the area of high pressure.

Although we cannot determine a concrete formation mechanism, we assume that at least frictional decoupling occurred at the coastline as a result of the seabreeze breakdown.

4 Conclusions and outlook

Low level jets that occurred during the OBLEX-F1 measuring campaing (May 2015 to September 2016) have been analysed. State-of-the-art remote sensing instruments, installed at FINO1, provided observational data. Despite the limited LiDAR data availability, the analyses give insight into LLJ characteristics. Supported by

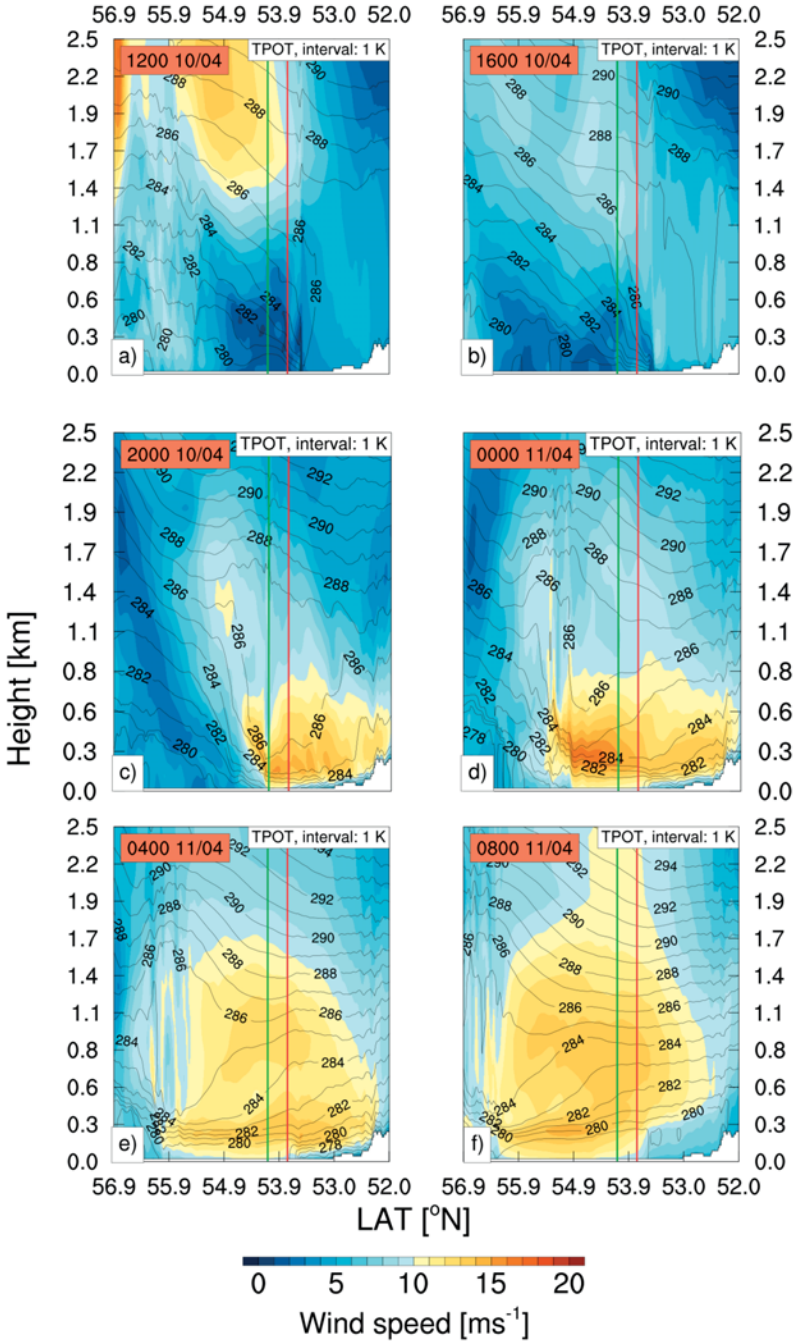

Figure 26: Overlay plot of wind speed (colored) and potential temperature (contour lines) evolution from LLJ 10/11 April 2016 at WRF cross section (3) shown in Figure 1, in a 135 degree angle in the crossing point of FINO1. The red line refers to the coastline position while the green line refers to the FINO1 position.

numerical simulations with the mesoscale atmospheric model WRF-ARW, possible formation mechanisms of LLJs above the Southern North Sea have been proposed.

It has been found that LLJs occurred on about 65 % of the days during the measuring campaign. No clear clustering of LLJ occurrences depending on months could be observed. The LLJs mainly occurred during the nighttime hours. Highest LLJ intensities tended to occur in the winter months. There was a moderate correlation for LLJ height and wind speed. With a median height of 236 m, the jet core heights were often in the range of modern offshore wind turbines. The core heights depended on the wind direction, with highest LLJ core heights for winds from the West and North-West sector and lowest LLJ core heights for winds from the North-East and South-East sector. The height also depended on the month, with higher LLJs during the winter months. Despite the prevailing wind direction at FINO1 is South-West, wind directions of LLJs were mainly between East over South-East to South. The wind direction of the LLJ depended on the month, as a clustering was observed for easterly and south-easterly wind during summer and spring and a clustering for West and South-West was observed during winter. Despite these findings, we

must mention, that the measurements might be biased by wake effects of surrounding wind farms, especially from Alpha Ventus during easterly wind directions. However, it is not an option to exclude winds from this sector in the analyses, as here the highest amounts of LLJs that come along with low heights and high wind shears, were found. Instead, the effects could be corrected with an algorithm such as proposed by Kinder et al. (2013). Alternatively, a more exposed site could be selected for future measuring campaigns. Apart from the obvious influence of wind farm wakes from easterly wind directions, it is expected, that measurements of LLJs during the winter, whose cores appear to occur more often at higher altitudes as well as more often during westerly wind directions, are less affected by this issue than easterly LLJs with lower core heights. However, these LLJs detected during winter time from westerly directions might also be a result of a misinterpretation by means of the detection algorithm. Another issue is, that wake effects are included in the measurements but not in the model output, what makes a model evaluation difficult. For future studies we recommend an application of a correction algorithm to address the wake effects at the FINO1 mast or to use WRF-LES simulations that include these wind farm wake effects.

Strong wind shears occurred during LLJs in our considered time period, with the highest values for air flows from North-West an South-East. In the considered case studies, extreme wind veers of up to 16°/100 m have been found. The wind speed maxima in both case studies were located below the temperature maxima. As surface friction is relatively low above the sea surface at FINO1 we hypothesize that the veering has a thermal origin in the investigated cases. We could not find clear dependencies of LLJ stability strength on season which was also a reason of the short time series of the bulk Richardson number. Furthermore, the bulk Richardson number is a proxy of atmospheric stability with relatively high uncertainties. By our used classification, mainly neutral conditions were found but with a slight tendency to higher values during spring. Earlier studies suggest, that air that is advected from above the land over the coastline towards the sea, leads to a stable ABL over the sea close to the coastline while the ABL stability decreases with travelled distance. This might explain the mainly neutral ABL conditions during LLJs in our study at FINO1, but this would need to be verified.

For a validation of our data analysis, we recommend time-continuous long-term LiDAR measurements at FINO1. However, due to the promising capability of WRF to capture LLJs over the Southern North Sea, a statistical analysis with data of numerical simulations from meso-scale models could, until then, provide appropriate results, as, for instance with data from the New European Wind Atlas (NEWA) (Petersen et al., 2013, 2014). Nevertheless, we experienced the well-known issue of wind shear underestimation by WRF in both case studies. We recommend further investigations that address this issue.

We suggest that LLJs above the Southern North Sea, especially during spring and summer, can be formed by different mechanisms:

1. Baroclinicity due to differential surface heating of land and sea surface
2. Baroclinicity due to fronts
3. Inertial oscillations induced by frictional decoupling that occurs

   a) at the coastline, b) as a consequence of ABL stabilization over land.

These mechanisms may interfere with each other. The LLJs appear to be correlated with the diurnal cycle. The dominating LLJ wind directions South-East and East support the baroclinicity hypothesis for a large amount of LLJs. Hence, favourable conditions are mainly given when an anticyclone is situated above Scandinavia and a cyclone is situated to its South-West which results in an easterly or southeasterly geostrophic flow. Under the aspect of the time-depending clustering of the wind directions mentioned above, we hypothesize, that these easterly LLJs occur mainly in spring, when stable boundary layers evolve above the sea or close to the coastline.

Therefore, we may divide LLJs under a seasonal aspect in:

1. LLJs in spring/summer, with relatively low core heights, mainly easterly wind directions and induced by baroclinicity and/or IOs and
2. LLJs in autumn/winter with higher core heights and more westerly wind directions. For these LLJs the formation mechanism is still unclear.

However this second type of LLJ is very speculative at this point as a stability criterion might filter out these detections during autumn and winter, as lower boundary layer stability is expected within these seasons compared to spring and summer. Due to the short length of time series of bulk Richardson numbers (January–April 2016) we cannot answer this question in our study. Furthermore, as highlighted, the stability can only be roughly estimated by means of the bulk Richardson number. Further research is recommended concerning this point.

Model results of one of the case studies suggest, that LLJs during easterly wind directions may merge with LLJs from the Baltic Sea above the Cimbrian Peninsula. As it appears that similarities in weather patterns exist, it could be of interest investigating potential interactions of LLJs, for instance, at sites in the Netherlands, Denmark or above the Baltic Sea.

Generally, a clear separation of all the different LLJ formation mechanisms could not be investigated at this time and might be an element of further studies. For a consequent investigation, a study which concentrates on the separation of these drivers would be desirable.

Idealized models can help to isolate the mechanisms. Furthermore, it could be an appropriate way to split the momentum budget equation from a model output during an LLJ to get an idea of the magnitude of each component as conducted by Rife et al. (2010).

Based on our findings and the high importance of the Southern North Sea for offshore wind energy purposes, we conclude, that LLJs can potentially have a high impact on wind energy and further research could contribute to finding solutions for adaptions on wind resources. To obtain clear climatological LLJ properties for this area, remote sensing measuring campaigns of larger temporal extent as well as at installations at different sites are suggested. Furthermore, wind forecasting applications considering LLJs, which may either be a wind power resource or a source of shear stress on turbine blades, can benefit from the knowledge of this study. Concerning the fast global warming due to a rise of atmospheric CO_2, a fast transition towards renewable energies is an urgent task. Our study can help making a step forward toward this target.

Acknowledgements

LiDAR and radiometer data were measured during the OBLEX-F1 field campaign that has been performed under the lead of the Norwegian Centre for Offshore Wind Energy (NORCOWE) funded by the Research Council of Norway (RCN 193821). The relevant instrumentation has been provided by the Offshore Boundary Layer Observatory (OBLO) project (project no. RCN 227777). Data storage is organized via the Norwegian e-infrastructure NorStore (project no. RCN: NS9060K). OBLEX-F1 was coordinated in collaboration between the University of Bergen (Geophysical Institute) and Christian Michelsen Research AS (project executing organisation) and actively supported by BSH, DEWI and FuE Kiel GmbH. The simulations were performed at the HPC Cluster EDDY, located at the University of Oldenburg (Germany) and funded by the Federal Ministry for Economic Affairs and Energy (Bundesministerium für Wirtschaft und Energie) under grant number 0324005. The authors thank the Project Management Jülich (PTJ) and the Federal Maritime And Hydrographic Agency (BSH) for providing access to the data of the offshore research platform FINO1. The work presented in this paper was also funded by the Ministry for Science and Culture of Lower Saxony through the funding initiative "Niedersächsisches Vorab" (Project Ventus Efficiens).

References

Andreas E.L., K.J. Claffy, A.P. Makshtas, 2000: Low-Level Atmospheric Jets And Inversions Over The Western Weddell Sea. – Bound.-Layer Meteor. **97**, 459–486, DOI: 10.1023/A:1002793831076.

Angevine, W.M., M. Tjernstroem, M. Žagar, 2006: Modeling of the coastal boundary layer and pollutant transport in New England. – J. Appl. Meteor. Climatol. **45**, 137–154, DOI: 10.1175/JAM2333.1.

Baas, P., F.C. Bosveld, H.K. Baltink, A.A.M. Holtslag, 2009: A climatology of nocturnal low-level jets at Cabauw. – J. Appl. Meteor. Climatol. **48**, 1627–1642, DOI: 10.1175/2009JAMC1965.1.

Baas, P., F.C. Bosveld, G. Lenderink, E. van Meijgaard, A.A.M. Holtslag, 2010: How to design single-column model experiments for comparison with observed nocturnal low-level jets. – Quart. J. Roy. Meteor. Soc. **136**, 671–684, DOI: 10.1002/qj.592.

Baas, P., B.J. van de Wiel, L. van den Brink and A. Holtslag, 2012: Composite hodographs and inertial oscillations in the nocturnal boundary layer. – Quart. J. Roy. Meteor. Soc. **138**, 528–535, DOI: 10.1002/qj.94.

Bakhoday Paskyabi, M., M. Flügge, J. Reuder, 2017: Air-Sea Interaction at Wind Energy Site in FINO1 Using DCF (Lidar) Measurements from OBLEX-F1 campaign. – EERA DeepWind2017, 14th Deep Sea Offshore Wind R & D, 2017-01-18–2017-01-20.

Banta R.M., Y.L. Pichugina, N.D. Kelley, R.M. Hardesty, W.A. Brewer, 2013: Wind Energy Meteorology: Insight into Wind Properties in the Turbine-Rotor Layer of the Atmosphere from High-Resolution Doppler Lidar. – Bull. Amer. Meteor. Soc. **94**, 883–902, DOI: 10.1175/BAMS-D-11-00057.1.

Beardsley, R.C., C.E. Dorman, C.A. Friehe, L.K. Rosenfeld, C.D. Winant, 1987: Local Atmospheric Forcing During the Coastal Ocean Dynamics Experiment 1. A Description of the Marine Boundary Layer and Atmospheric Conditions Over a Northern California Upwelling Region. – J. Geophys. Res. Oceans **92**, 1467–1488, DOI: 10.1029/JC092iC02p01467.

Beeken, A., T. Neumann, 2008: Five Years of Offshore Measurements at the Fino1 Platform in the German Bight. – DEWI Magazin **33**, 6–11.

Blackadar, A.K., 1957: Boundary Layer Wind Maxima and Their Significance for the Growth of Nocturnal Inversions. – Bull. Amer. Meteor. Soc. **38**, 283–290.

Bonner, W.D., 1968: Climatology of the Low Level Jet. – Mon. Wea. Rev. **96**, 833–850, DOI: 10.1175/1520-0493(1968)096<0833:COTLLJ>2.0.CO;2.

Burk, S.D., W.T. Thompson, 1996: The summertime low-level jet and marine boundary layer structure along the California coast. – Mon. Wea. Rev. **124**, 668–686, DOI: 10.1175/1520-0493(1996)124<0668:TSLLJA>2.0.CO;2.

Chen, R., L. Tomassini, 2015: The Role of Moisture in Summertime Low-Level Jet Formation and Associated Rainfall over the East Asian Monsoon Region. – J. Atmos. Sci. **72**, 3871–3890, DOI: 10.1175/JAS-D-15-0064.1.

Cherukuru N.W., R. Calhoun, R. Krishnamurthy, B. Svardal, J. Reuder, M. Flügge, 2017: 2D VAR single Doppler lidar vector retrieval and its application in offshore wind energy. – Energy Procedia, **137**, 497–504, DOI: 10.1016/j.egypro.2017.10.378.

Churnside J.H., T.A. Stermitz, J.A. Schroeder, 1994: Temperature Profiling with Neural Network Inversion of Microwave Radiometer Data. – J. Atmos. Ocean. Technol., **11**, 105–109, DOI: 10.1175/1520-0426(1994)011<0105:TPWNNI>2.0.CO;2.

Coffer, B.E., M.D. Parker, 2015: Impacts of Increasing Low-Level Shear on Supercells during the Early Evening Transition. – Mon. Wea. Rev. **143**, 1945–1969, DOI: 10.1175/MWR-D-14-00328.1.

Colle, B.A., D.R. Novak, 2010: The New York Bight Jet: Climatology and Dynamical Evolution. – Mon. Wea. Rev. **138**, 2385–2404, DOI: 10.1175/2009MWR3231.1.

Dee, D.P., S.M. Uppsala, A.J. Simmons, P. Berrisford, P. Poli, S. Kobayashi, U. Andrae, M.A. Balmaseda, G. Balsamo, P. Bauer, P. Bechtold, A.C.M Beljaars, L. van de Berg, J. Bidlot, N. Bormann, C. Delsol, R. Dragani, M. Fuentes, A.J. Geer, L. Haimberger, S.B. Healy, H. Hersbach, E.V. Hólm, L. Isaksen, P. Kållberg, M. Köhler, M. Matricardi, A.P. Mcnally, B.M. Monge-Sanz, J.J. Morcrette, B.K. Park and C. Peubey, P. de Rosnay, C. Tavolato, J.N. Thépaut, F. Vitart, 2011: The ERA-Interim reanalysis: Configuration and performance of the data assimilation system. – Quart. J. Roy. Meteor. Soc. **137**, 553–597, DOI: 10.1002/qj.828.

Donlon, C.J., M. Martin, J. Stark, J. Roberts-Jones, E. Fiedler, W. Wimmer 2012: The Operational Sea Surface Temperature and Sea Ice Analysis (OSTIA) system. – Remote Sens. Env. **116**, 140–158, DOI: 10.1016/j.rse.2010.10.017.

Dörenkämper, M., 2015: An investigation of the atmospheric influence on spatial and temporal power fluctuations in offshore wind farms. – PhD Thesis, University of Oldenburg, München, Verlag Dr. Hut.

Dörenkämper, M., M. Optis, A. Monahan, G. Steinfeld, 2015a: On the Offshore Advection of Boundary-Layer Structures and the Influence on Offshore Wind Conditions. – Bound.-Layer Meteor. **155**, 459–482, DOI: 10.1007/s10546-015-0008-x.

Dörenkämper, M., B. Witha, G. Steinfeld, D. Heinemann, M. Kühn, 2015b: The impact of stable atmospheric boundary layers on wind-turbine wakes within offshore wind farms. – J. Wind. Eng. Ind. Aerodyn. **144**, 146–153, DOI: 10.1016/j.jweia.2014.12.011.

Dudhia, J., 1989: Numerical Study of Convection Observed during the Winter Monsoon Experiment Using a Mesoscale Two-Dimensional Model. – J. Atmos. Sci. **46**, 3077–3107, DOI: 10.1175/1520-0469(1989)046<3077:NSOCOD>2.0.CO;2.

Emeis, S., 2013: Wind Energy Meteorology. – Springer-Verlag Berlin Heidelberg, 196 pp., DOI: 10.1007/978-3-642-30523-8.

Emeis, S., 2014: Wind speed and shear associated with low-level jets over Northern Germany. – Meteorol. Z. **23**, 295–304, DOI: 10.1127/0941-2948/2014/0551.

Fligg, A., 2017: Validation of remotely sensed temperature and humidity profiles against radiosoundings. – Master's thesis, University of Oldenburg, Germany.

Floors, R., C.L. Vincent, S. Gryning, A. Peña, E. Batchvarova, 2013: The Wind Profile in the Coastal Boundary Layer: Wind Lidar Measurements and Numerical Modelling. – Bound.-Layer Meteor. **147**, 469–491, DOI: 10.1007/s10546-012-9791-9.

Floors, R., A. Peña, S.E. Gryning, 2015: The effect of baroclinicity on the wind in the planetary boundary layer. – Quart. J. Roy. Meteor. Soc. **141**, 619–630, DOI: 10.1002/qj.2386.

Fraunhofer IEE, 2018: Windmonitor. – Published online: http://windmonitor.iee.fraunhofer.de/ (accessed at 06.07.2018).

Grell, G.A., 1993: Prognostic Evaluation of Assumptions Used by Cumulus Parameterizations. – Mon. Wea. Rev. **121**, 764–787, DOI: 10.1175/1520-0493(1993)121<0764:PEOAUB>2.0.CO;2.

Grell, G., D. Devenyi, 2002: A generalized approach to parameterizing convection combining ensemble and data assimilation techniques. – Geophys. Res. Lett. **29**, published online, DOI: 10.1029/2002GL015311.

Gutierrez, W., G. Araya, P. Kiliyanpilakkil, A. Ruiz-Columbie, M. Tutkun, Castillo, L., 2016: Structural impact assessment of low level jets over wind turbines. – J. Ren. Sustain. Energy **8**, 023308, DOI: 10.1063/1.4945359.

Gutierrez, W., A. Ruiz-Columbie, M. Tutkun., L. Castillo, 2017: Impacts of the low-level jet's negative wind shear on the wind turbine, – Wind Energ. Sci. **2**, 533–545, DOI: 10.5194/wes-2-533-2017.

Haurwitz, B., 1947: Comments on the Sea-Breeze Circulation. – J. Meteor. **4**, 1–8, DOI: 10.1175/1520-0469(1947)004<0001:COTSBC>2.0.CO;2.

Helmis, C.G., Q. Wang, G. Sgouros, S. Wang, C. Halios, 2013: Investigating the Summertime Low-Level Jet Over the East Coast of the U.S.A.: A Case Study. – Bound.-Layer Meteor. **149**, 259–276, DOI: 10.1007/s10546-013-9841-y.

Högström, U., A.S. Smedman-Högström, 1984: The wind regime in coastal areas. – Bound.-Layer Meteor. **30**, 351–373, DOI: 10.1007/BF00121961.

Holton, J.R., 1967: The diurnal boundary layer wind oscillation above sloping terrain. – Tellus **19**, 199–205, DOI: 10.3402/tellusa.v19i2.9766.

Hoxit, L.R., 1974: Planetary Boundary Layer Winds in Baroclinic Conditions. – J. Atmos. Sci. **31**, 1003–1020, DOI: 10.1175/1520-0469(1974)031<1003:PBLWIB>2.0.CO;2.

Joffre, S.M., 1982: Assessment of the separate effects of baroclinicity and thermal stability in the atmospheric boundary layer over the sea. – Tellus **34**, 567–578, DOI: 10.1111/j.2153-3490.1982.tb01845.x.

Källstrand, B., 1998: Low Level Jets in a Marine Boundary Layer During Spring. – Contrib. Atmos. Phys. **71**, 359–373.

Kalverla, P.C., G.J. Steeneveld, R.J. Ronda, A.A.M. Holtslag, 2017: An observational climatology of anomalous wind events at offshore meteomast IJmuiden (North Sea). – Wind. Eng. Ind. Aerodyn. **165**, 86–99, DOI: 10.1016/j.jweia.2017.03.008.

Kinder, F., A. Westerhellweg, T. Neumann, 2013: Park Correction for FINO1 Wind Speed Measurements at alpha ventus. – DEWI Magazin **42**, 61–64.

Kleczek, M.A., G.J. Steeneveld, A.A.M. Holtslag, 2014: Evaluation of the Weather Research and Forecasting Mesoscale Model for GABLS3: Impact of Boundary-Layer Schemes, Boundary Conditions and Spin-Up. – Bound.-Layer Meteor. **152**, 213–243, DOI: 10.1007/s10546-014-9925-3.

Krishnamurthy, R., J. Reuder, B. Svardal, H.J.S. Fernando, J.B. Jakobsen, 2017: Offshore Wind Turbine Wake characteristics using Scanning Doppler Lidar. –Energy Procedia, **137**, 428–442, DOI: 10.1016/j.egypro.2017.10.367.

Krogsæter, O., J. Reuder, 2015: Validation of boundary layer parameterization schemes in the Weather Research and Forecasting Model (WRF) under the aspect of offshore wind energy applications – Part II: Boundary layer height and atmospheric stability. – Wind Energy **18**, 1291–1302, DOI: 10.1002/we.1765.

Kumer, V.M., J. Reuder, B.R. Furevik, 2014: A comparison of LiDAR and radiosonde wind measurements. – Energy Procedia **53**, 214–220, DOI: 10.1016/j.egypro.2014.07.230.

Lettau, H., 1954: A study of the mass, momentum and energy budget of the atmosphere. – Meteor. Atmos. Phys. **7**, 133–157, DOI: 10.1007/BF02277912.

Lee, A.J., 1980: North Sea: Physical Oceanography. The North-West European Shelf Seas: The Sea Bed and the Sea in Motion II. – Phys. Chem. Ocean. Phys. Res.**24**, 467–493.

Lee, J.A., J.P. Hacker, L. Delle Monache, B. Kosović, A. Clifton, F. Vandenberghe, J.S. Rodrigo, 2017: Improving Wind Predictions in the Marine Atmospheric Boundary Layer through Parameter Estimation in a Single-Column Model. – Mon. Wea. Rev. **145**, 5–24, DOI: 10.1175/MWR-D-16-0063.1.

Lundquist, J.K., 2003: Intermittent and Elliptical Inertial Oscillations in the Atmospheric Boundary Layer. – J. Atmos. Sci. **60**, 2661–2673, DOI: 10.1175/1520-0469(2003)060<2661:IAEIOI>2.0.CO;2.

Mahrt, L., D. Vickers, E.L. Andreas, 2014.: Low-level wind maxima and structure of the stably stratified boundary layer in the coastal zone. – J. Appl. Meteor. Climatol. **53**, DOI: 10.1175/JAMC-D-13-0170.1.

Martin, J.E., 2006: Mid-Latitude Atmospheric Dynamics: A First Course. – John Wiley & Sons, Ltd, 336 pp.

Mlawer Eli,. J., S.J. Taubman, P.D. Brown, M.J. Iacono, S.A. Clough, 1997: Radiative transfer for inhomogeneous atmospheres: RRTM, a validated correlated-k model for the longwave. – J. Geophys. Res. Atmos. **102**, 16663–16682, DOI: 10.1029/97JD00237.

Nakanishi, M., H. Niino, 2006: An improved Mellor-Yamada Level-3 model: Its numerical stability and application to a regional prediction of advection fog. – Bound.-Layer Meteor. **119**, 397–407, DOI: 10.1007/s10546-005-9030-8.

Neumann, T., K. Nolopp, M. Strack, H. Mellinghoff, H. Söker, E. Mittelstaedt, W.J. Gerasch, G. Fischer, 2003: Erection of German offshore measuring platform in the North Sea. – DEWI Magazin **23**, 32–46.

Neumann, T., K. Nolopp, V. Riedel, M. Strack, K. Herklotz, J. Stein, 2004: Assessment of One Year Wind Measurements on the First Offshore Wind Research Platform in the German Bight – FINO1. – DEWEK 2004 Conference Paper, 1–4.

Nunalee, C.G., S. Basu, 2013: Mesoscale modeling of coastal low-level jets: implications for offshore wind resource estimation. – Wind Energy **17**, DOI: 10.1002/we.

Nunalee, C., S. Basu, 2014: Mesoscale Modeling of Low-Level Jets over the North Sea. –In: Hoelling M., J. Peinke, S. Ivanell (Eds): Wind Energy – Impact of Turbulence. – Research Topics in Wind Energy, vol 2. Springer, Berlin, Heidelberg, 197–202, DOI: 10.1007/978-3-642-54696-9_29.

Petersen, E.L., I. Troen, H. Ejsing Jörgensen, J. Mann, 2013: Are local wind power resources well estimated? – Env. Res. Lett. **8**, 011005.

Petersen, E.L., I. Troen, H. Ejsing Jörgensen, J. Mann, 2014: The new European wind atlas. – Energy Bull. **17**, 34–39.

Peña, A., S.E. Gryning, R. Floors, 2014: The turning of the wind in the atmospheric boundary layer. – J. Phys.: Conf. Ser. **524**, 012118, DOI: 10.1088/1742-6596/524/1/012118.

Platis, A., S.K. Siedersleben, J. Bange, A. Lampert, K. Baerfuss, R. Hankers, B. Canadillas, R. Foreman, J. Schulz-Stellenfleth, B. Djath, T. Neumann, S. Emeis, 2018: First in situ evidence of wakes in the far field behind offshore wind farms. – Sci. Rep. **8**, DOI: 10.1038/s41598-018-20389-y.

Radiometer Physics, 2015: Instrument Operation and Software Guide. – Technical Report 01/10.

Rife D.L., J.O. Pinto, A.J. Monaghan, C.A. Davis, J.R. Hannan, (2010): Global distribution and characteristics of diurnally varying low-level jets. – J. Climate **23**, 5041–5064, DOI: 10.1175/2010JCLI3514.1.

Shapiro A., Fedorovich, E., S. Rahimi, 2016: A Unified Theory for the Great Plains Nocturnal Low-Level Jet. – J. Atmos.c Sci. **73**, 3037–3057, DOI: 10.1175/JAS-D-15-0307.1.

Skamarock, W.C., J.B. Klemp, J. Dudhia, D.O. Gill, D.M. Barker, M.G. Duda, X.Y. Huang, Wang W., J.G. Powers, 2008: A Description of the Advanced Research WRF Version 3. – Technical Report **113**, DOI: 10.5065/D68S4MVH.

Smedman, A.S., M. Tjernström, U. Högström, 1993: Analysis of the turbulence structure of a marine low-level jet. – Bound.-Layer Meteor. **66**, 105–126, DOI: 10.1007/BF00705462.

Smedman, A.S., H. Bergström, U. Bergström, 1995: Spectra, variances and length scales in a marine stable boundary layer dominated by a low level jet. – Bound.-Layer Meteor. **76**, 211–232, DOI: 10.1007/BF00709352.

Smedman, A.S., U. Högström, H. Bergström, 1996: Low Level Jets – A Decisive Factor for Off-Shore Wind Energy Siting in the Baltic Sea. – Wind Engineering **20**, 137–147.

Smedman, A.S., H. Bergström, B. Grisogono, 1997a: Evolution of stable internal boundary layers over a cold sea. – J. Geophys. Res. Oceans **102**, 1091–1099, DOI: 10.1029/96JC02782.

Smedman, A.S., U. Högström, H. Bergström, 1997b: The turbulence regime of a very stable marine airflow with quasi-frictional decoupling. – J. Geophys. Res. Oceans **102**, 21049–21059, DOI: 10.1029/97JC01070.

Soares, P.M.M., R.M. Cardoso, A. Semedo, M.J. Chinita, R. Ranjha, 2014: Climatology of the Iberia coastal low-level wind jet: Weather research forecasting model high-resolution results. – Tellus, Series A: Dynamic Meteorology and Oceanography **66**, 22377, DOI: 10.3402/tellusa.v66.22377.

Song, J., K. Liao, R.L. Coulter, B.M. Lesht, 2005: Climatology of the Low-Level Jet at the Southern Great Plains Atmospheric Boundary Layer Experiments Site. – J. Appl. Meteor. Climatol. **44**, 1593–1606, DOI: 10.1175/JAM2294.1.

Stauffer, D.R., N.L. Seaman, 1994: Multiscale four-dimensional data assimilation. – J. Appl. Meteor. Climatol. **33**, 416–434, DOI: 10.1175/1520-0450(1994)033<0416:MFDDA>2.0.CO;2.

Storm B., J. Dudhia, S. Basu, A. Swift, I. Giammanco, 2009: Evaluation of the Weather Research and Forecasting model on forecasting low-level jets: implications for wind energy. – Wind Energ. **12**, 81–90, DOI: 10.1002/we.288.

Stull, R.B., 1988: An Introduction to Boundary Layer Meteorology. – Kluwer Academic Publishers, 670 pp.

Svensson, N., H. Bergström, E. Sahlée, A. Rutgersson, 2016: Stable atmospheric conditions over the Baltic Sea: model evaluation and climatology. – Boreal Env. Res. **21**, 387–404.

Tewari, M.F., F. Chen, W. Wang, J. Dudhia, M.A. LeMone, K. Mitchell, M. Ek, G. Gayno, J. Wegiel, R.H. Cuenca, 2004: Implementation and Verification of the Unified NOAH Land Surface Model in the WRF Model. – 20th Conference on Weather Analysis and Forecasting. 16th Conference on Numerical Weather Prediction, Seattle, 11–15.

Thompson, G., P.R. Field, R.M. Rasmussen, W.D. Hall, 2008: Explicit Forecasts of Winter Precipitation Using an Improved Bulk Microphysics Scheme. Part II: Implementation of a New Snow Parameterization. – Mon. Wea. Rev. **136**, 5095–5115, DOI: 10.1175/2008MWR2387.1.

Tuononen, M., H.A. Sinclair, T. Vihma, 2015: A climatology of low-level jets in the mid-latitudes and polar regions of the Northern Hemisphere. – Atmos. Sci. Lett. **16**, 492–499, DOI: 10.1002/asl.587.

Van De Wiel, B.J.H., A.F. Moene, G.J. Steeneveld, P. Baas, F.C. Bosveld, A.A.M. Holtslag, 2010: A Conceptual View on Inertial Oscillations and Nocturnal Low-Level Jets. – J. Atmos. Sci. **67**, 2679–2689. DOI: 10.1175/2010JAS3289.1.

Vanderwende B.J., J.K. Lundquist, M.E. Rhodes, E.S. Takle, S.L. Irvin, 2015: Observing and Sim-

ulating the Summertime Low-Level Jet in Central Iowa. – Mon. Wea. Rev. **143**, 2319–2336, DOI: 10.1175/MWR-D-14-00325.1.

Wagner, R., M. Courtney, 2010: Accounting for the speed shear in wind turbine power performance measurement. – Roskilde: Risø National Laboratory for Sustainable Energy, (Risø-PhD No. 58(EN)).

Werkhoven, E.J., J.P. Verhoef, 2012: Offshore Meteorological Mast IJmuiden – Abstract of Instrumentation Report. – Technical report.

Westerhellweg, A., T. Neumann, V. Riedel, 2012: FINO1 Mast Correction. – DEWI Magazin **40**, 60–66.

Yang, B., Y. Qian, L.K. Berg, P.L. Ma, S. Wharton, V. Bulaevskaya, H. Yan, Z. Hou, W.J. Shaw, 2016: Sensitivity of Turbine-Height Wind Speeds to Parameters in Planetary Boundary-Layer and Surface-Layer Schemes in the Weather Research and Forecasting Model. – Bound. Layer Meteor. **162**, 1–26, DOI: 10.1007/s10546-016-0185-2.